Cerebral Cortex, October 2015;25: 3723–3742

doi: 10.1093/cercor/bhu246
Advance Access Publication Date: 19 October 2014
ORIGINAL ARTICLE

ORIGINAL ARTICLE

Identifying and Mapping Connectivity Patterns of Brain Network Hubs in Alzheimer's Disease

Zhengjia Dai[1,2], Chaogan Yan[1,3], Kuncheng Li[4], Zhiqun Wang[4], Jinhui Wang[1], Miao Cao[1,2], Qixiang Lin[1,2], Ni Shu[1,2], Mingrui Xia[1,2], Yanchao Bi[1,2], and Yong He[1,2]

[1]State Key Laboratory of Cognitive Neuroscience and Learning & IDG/McGovern Institute for Brain Research, [2]Center for Collaboration and Innovation in Brain and Learning Sciences, Beijing Normal University, Beijing 100875, China, [3]Nathan Kline Institute for Psychiatric Research, Orangeburg, NY 10962, USA and [4]Department of Radiology, Xuanwu Hospital of Capital Medical University, Beijing 100053, China

Address correspondence to Yong He, PhD, State Key Laboratory of Cognitive Neuroscience and Learning & IDG/McGovern Institute for Brain Research, and Center for Collaboration and Innovation in Brain and Learning Sciences, Beijing Normal University, Beijing 100875, China. Email: yong.he@bnu.edu.cn

Abstract

Alzheimer's disease (AD) is associated not only with regional gray matter damages, but also with abnormalities in functional integration between brain regions. Here, we employed resting-state functional magnetic resonance imaging data and voxel-based graph-theory analysis to systematically investigate intrinsic functional connectivity patterns of whole-brain networks in 32 AD patients and 38 healthy controls (HCs). We found that AD selectively targeted highly connected hub regions (in terms of nodal functional connectivity strength) of brain networks, involving the medial and lateral prefrontal and parietal cortices, insula, and thalamus. This impairment was connectivity distance-dependent (Euclidean), with the most prominent disruptions appearing in the long-range connections (e.g., 100–130 mm). Moreover, AD also disrupted functional connections within the default-mode, salience and executive-control modules, and connections between the salience and executive-control modules. These disruptions of hub connectivity and modular integrity significantly correlated with the patients' cognitive performance. Finally, the nodal connectivity strength in the posteromedial cortex exhibited a highly discriminative power in distinguishing individuals with AD from HCs. Taken together, our results emphasize AD-related degeneration of specific brain hubs, thus providing novel insights into the pathophysiological mechanisms of connectivity dysfunction in AD and suggesting the potential of using network hub connectivity as a diagnostic biomarker.

Key words: connectome, functional connectivity, graph theory, module, PCC/PCu

Introduction

Alzheimer's disease (AD) is a progressive, neurodegenerative disease characterized by a decline of memory and cognitive functions. The prevailing β-amyloid (Aβ)-cascade hypothesis of AD pathophysiology suggests that interstitial Aβ proteins exert a toxic effect on surrounding neurons and synapses, thereby disturbing their functions (Hardy and Selkoe 2002; Selkoe 2008). Indeed, recent research suggests that, prior to neuronal death and atrophy, disruption of functional connectivity between regions may represent an early deleterious outcome of Aβ proteins in AD (Gili et al. 2011; Sheline and Raichle 2013). Even before the stage of aggregation of Aβ fragments into amyloid plaques, there is a dysfunction of synaptic transmission in many brain areas due to dimers or even monomers from the Aβ cascade (for review, see D'Amelio and Rossini 2012).

Resting-state functional MRI (R-fMRI) is a promising neuroimaging technique that can non-invasively measure spontaneous or intrinsic brain activity (Biswal et al. 1995). R-fMRI has been widely used to study inter-regional functional connectivity in healthy and diseased populations (for reviews, see Fox and Raichle 2007; Kelly et al. 2012), particularly with the capability of detecting subtle connectivity abnormalities in early AD (Jack et al. 2010; Sperling et al. 2011; Sheline and Raichle 2013). Recently, the combination of R-fMRI and graph-based network analysis allows revealing the topological organization of human whole-brain functional networks, such as small-world attributes and network modularity (for reviews, see Bullmore and Sporns 2009; He and Evans 2010; Wang et al. 2010). An important and convergent finding is that human brain functional networks contain a small number of hubs with disproportionately numerous connections (Achard et al. 2006; Buckner et al. 2009; He et al. 2009; Tomasi and Volkow 2010). These brain hubs, primarily located in the medial and lateral frontal and parietal cortices, have higher rates of cerebral blood flow, aerobic glycolysis, and oxidative glucose metabolism, and play vital roles in supporting fast communication across brain regions (Vaishnavi et al. 2010; Liang et al. 2013; Tomasi et al. 2013).

Recent research suggests that the brain hubs may be preferentially affected in AD. Buckner et al. (2009) have demonstrated that the functional hubs of healthy human brains have a striking overlap with regions showing higher Aβ deposition in patients with AD. de Haan, Mott, et al. (2012) employed a computational model to test the activity-dependent degeneration hypothesis that hub vulnerability in AD could be due to the high-level continuous baseline activity and/or associated metabolism. In mouse brains, the amount of Aβ in the interstitial fluid and the development of amyloid plaques are associated with synaptic activity (Selkoe 2006; Bero et al. 2011, 2012). These findings suggest that the brain hubs tend to have amyloid plaque deposition that leads to functional disconnections among regions. Previous R-fMRI studies reported AD-related changes in the topological architecture of whole-brain functional networks, such as the loss of small-worldness, modular disorganization, and regional dysconnectivity (Supekar et al. 2008; Sanz-Arigita et al. 2010; Liu et al. 2013; for reviews, see Xie and He 2011; Tijms et al. 2013). However, the connectivity patterns of brain hubs in R-fMRI networks in AD remain to be elucidated.

Many studies suggest that much of the brain's massive metabolic cost is attributable to the active maintenance of electrochemical gradients across neuronal membranes, which is required to support signaling and coordination of neuronal activity at anatomically separated regions (Attwell and Laughlin 2001; Niven and Laughlin 2008). The brain metabolic costs increase in proportion to the total surface area of the neuronal membrane. Thus, these costs are a function of axonal length and diameter, which are 2 key factors to determine the area of the neuronal membrane, with longer distance connections being metabolically more expensive to maintain (Karbowski 2007). Direct evidence also suggests that the metabolic costs of brain regions are closely associated with inter-regional connectivity distance: Long-range brain hubs consume more energy than short-range hubs (Sepulcre et al. 2010; Liang et al. 2013). Specifically, several recent studies have paid more attention to the topology of anatomically embedded brain networks and highlighted the importance of connectivity distances on brain network organization (Vértes et al. 2012; Alexander-Bloch et al. 2013). Relating to AD research, long-range brain hubs with increased metabolic cost may generate more Aβ deposition and lead to more serious functional disconnections. However, very few studies have directly examined whether patients with AD are mainly associated with longer distance disconnections, or AD-related disruption of brain hubs is connection-distance-dependent.

Here, we used R-fMRI and voxel-based graph analysis approaches to comprehensively investigate AD-related changes in the functional hubs of whole-brain networks. Such a voxel-wise approach avoids parcellation-dependent effects on the topological organization of brain networks (Smith et al. 2011; de Reus and van den Heuvel 2013). We sought to determine (1) whether patients with AD show disrupted hub connectivity patterns in their whole-brain functional networks and whether this disruption is connection-distance-dependent, and (2) if so, whether these topological changes in functional hubs significantly correlate with the behavioral characteristics of AD and may serve as valuable biomarkers for disease classification.

Materials and Methods

Participants

Seventy-five right-handed subjects (34 AD patients and 41 healthy controls, HCs) participated in this study. The AD patients were recruited from individuals who consulted a memory clinic at the Xuanwu Hospital with memory complaints. The HCs were recruited through advertisement from the local community. All participants were assessed clinically with the Clinical Dementia Rating (CDR) score (Morris 1993) to be categorized as HCs (CDR = 0) or as patients in the early stages of AD (18 patients with CDR = 1 and 16 patients with CDR = 0.5). The patients were given routine drug treatment (donepezil, memantine, and/or rivastigmine tartrate). All HCs had no history of neurological or psychiatric disorders, sensorimotor impairment or cognitive complaints, no abnormal anatomical findings by conventional brain MRI, and had mini-mental state examination (MMSE) scores of 28 or higher. All participants underwent a complete physical and neurological examination, standard laboratory tests, and neuropsychological assessments, which included the MMSE, Montreal Cognitive Assessment (MoCA), Extended Scale for Dementia (ESD), World Health Organization–University of California–Los Angeles Auditory Verbal Learning Test (AVLT), Clock Drawing Task (CDT), Activity of Daily Living Scale (ADL), Functional Activities Questionnaire (FAQ), Hamilton Depression Scale, and Hachinski Ischemic Score. The diagnosis of AD fulfilled the new research criteria for possible or probable AD (Dubois et al. 2007, 2010; McKhann et al. 2011). Of these cognitive measures, MMSE, MoCA, and ESD are comprehensive cognitive screeners that cover a wide range of cognitive functions, with MMSE being one of the most influential standardized cognitive state examination tools and screener of AD, MoCA screening for dysfunctions of attention, executive function, memory, language, visual, abstract thinking, structure calculation and directional force, and ESD testing the ability associated with learning, attention, memory, calculation, abstraction, understanding, structure, language fluency, object use, and recognition. AVLT is commonly used to test events memory function. CDT is used to test executive function. These cognitive measures are frequently used in the studies of AD and higher scores indicate better performance. Written informed consent was obtained from each participant, and this study was approved by the Medical Research Ethics Committee of Xuanwu Hospital, Beijing, China. The data of 2 AD patients (CDR = 0.5) and 3 HCs were discarded due to the failure of imaging normalization (see Image Preprocessing). The dataset has been used previously to study seed-based functional connectivity in the medial and lateral parietal subregions in AD (Wang, Xia, et al. 2013; Xia et al. 2014).

A subset of the dataset (16 AD patients and 22 HCs) was also used to study regional brain activity in AD (Wang, Yan, et al. 2011; Dai et al. 2012). Clinical and demographic data of the remaining 70 participants are summarized in Table 1.

MRI Acquisition

All participants were scanned on a Siemens 3-T Magnetom Sonata scanner (Siemens, Erlangen, Germany). Foam pads and headphones were used to minimize head movement and scanner noise. Functional images were collected axially using an echo-planar imaging sequence: repetition time (TR)/echo time (TE) = 2000 ms/40 ms, flip angle (FA) = 90°, field of view (FOV) = 240 × 240 mm^2, matrix = 64 × 64, slices = 28, thickness = 4 mm, voxel size = 3.75 × 3.75 × 4 mm^3, gap = 1 mm, and bandwidth = 2232 Hz/pixel. Prior to the scan, the subjects were instructed to keep their eyes closed but not fall asleep, relax their minds, and move as little as possible during data acquisition. The scan lasted for 478 s and thus included 239 functional volumes for each subject. A simple questionnaire indicated that all of the subjects had not fallen asleep during the scan. Three-dimensional T_1-weighted magnetization-prepared rapid gradient echo (MPRAGE) sagittal images were also obtained using the following sequence: TR/TE = 1900 ms/2.2 ms, FA = 9°, inversion time = 900 ms, FOV = 256 × 256 mm^2, matrix = 256 × 256, slices = 176, thickness = 1 mm, and voxel size = 1 × 1 × 1 mm^3.

Image Preprocessing

Unless otherwise stated, all functional imaging data preprocessing was carried out using Statistical Parametric Mapping (SPM8, http://www.fil.ion.ucl.ac.uk/spm) and Data Processing Assistant for Resting-State fMRI (DPARSF; Yan and Zang 2010). Briefly, the first 10 functional volumes were discarded to allow for stabilization of the initial signal and adaptation of the participants to the circumstances. The remaining fMRI images were then corrected for acquisition time delay between slices and further realigned to the first volume to correct for head motion. No subject was excluded under a head motion criterion of 3 mm and 3°. The individual T_1-weighted images were coregistered to the mean functional image after motion correction using a linear transformation (Collignon et al. 1995) and were then segmented into gray matter (GM), white matter, and cerebrospinal fluid tissue maps with SPM's a priori tissue maps as reference by using a unified segmentation algorithm (Ashburner and Friston 2005). The resultant GM, white matter, and cerebrospinal fluid images were further nonlinearly registered into the Montreal Neurological Institute (MNI) space with the information estimated in unified segmentation and then averaged across all subjects to create custom GM, white matter, and cerebrospinal fluid templates. Next, the coregistered T_1 images were segmented again with custom tissue templates as reference images using the unified segmentation algorithm (Ashburner and Friston 2005). Such a custom template-based registration procedure allowed reducing the inaccuracy of the spatial normalization of functional volumes due to GM atrophy in the elderly population. We then applied the transformation parameters estimated during unified segmentation to the motion-corrected functional volumes and resampled the transformational functional images to 3-mm isotropic voxels that are the minimum spatial resolution capturing cortical folding (Kiselev et al. 2003) and reflect neuronal patterns of columnar grain (Kriegeskorte et al. 2010). The data of 5 subjects (2 AD and 3 HCs) were excluded from further analysis because of the failure of imaging normalization that might be caused by severe GM atrophy or image artifacts. The normalized functional images further underwent spatial smoothing with a 4-mm full width at half maximum (FWHM) Gaussian kernel and removal of linear trends. Temporal band-pass filtering (0.01–0.1 Hz) was performed on the time series of each voxel using the Resting-State fMRI Data Analysis Toolkit (Song et al. 2011) to reduce the effect of low-frequency drifts and high-frequency physiological noise (Biswal et al. 1995; Lowe et al. 1998). Finally, the nuisance signals (6 head motion parameters, global signal, cerebrospinal fluid, and white matter signals) were regressed out from each voxel's time course. The residuals were used for the following resting-state functional connectivity analysis.

Nodal Functional Connectivity Strength Analysis

To identify the hub regions of the whole-brain network, we performed a nodal functional connectivity strength (FCS) analysis as follows. First, for each participant, we computed functional

Table 1 Demographic and neuropsychological data of AD patients and HCs

	AD (n = 32)	HC (n = 38)	P-value
Age (years)	52–86 (71.25 ± 8.63)	50–86 (68.39 ± 7.78)	0.15[a]
Gender (M/F)	14/18	13/25	0.41[b]
Education (years)	5–16 (9.75 ± 3.14)	5–16 (9.95 ± 3.44)	0.80[a]
CDR	0.5 (n = 14), 1 (n = 18)	0	–
MMSE	10–25 (18.56 ± 3.99)	28–30 (28.63 ± 0.67)	<0.001[a]
MoCA	8–19 (14.94 ± 3.23)	27–30 (28.63 ± 0.79)	<0.001[a]
ESD	107–200 (155.33 ± 26.48)	180–248 (227.74 ± 15.68)	<0.001[a]
AVLT	8–24 (14.81 ± 4.12)	39–52 (44.42 ± 2.74)	<0.001[a]
CDT	3–8 (6.13 ± 1.43)	8–9 (8.71 ± 0.46)	<0.001[a]
ADL	22–45 (30.41 ± 7.21)	20–22 (21.08 ± 0.78)	<0.001[a]
FAQ	4–11 (6.25 ± 1.70)	0–2 (0.55 ± 0.76)	<0.001[a]
HAMD	0–3 (1.06 ± 1.08)	0–3 (0.61 ± 1.00)	0.07[a]
HIS	0–3 (1.16 ± 0.77)	0–3 (1.13 ± 1.07)	0.91[a]

Note: Data are presented as the range of minimum–maximum (mean ± SD).
AD, Alzheimer's disease; HC, healthy control; CDR, Clinical Dementia Rating; MMSE, Mini-Mental State Examination; MoCA, Montreal Cognitive Assessment; ESD, The Extended Scale for Dementia; AVLT, World Health Organization–University of California–Los Angeles Auditory Verbal Learning Test; CDT, Clock Drawing Task; ADL, Activity of Daily Living Scale; FAQ, Functional Activities Questionary; HAMD, Hamilton Depression Scale; HIS, Hachinski Ischemic Score.
[a]The P-value was obtained by the two-sample two-tailed t-test.
[b]The P-value was obtained by the two-tailed Pearson χ^2 test.

connectivities by estimating Pearson's correlations between the time series of any pairs of brain voxels, resulting in an individual whole-brain functional connectivity matrix. This procedure was constrained within a GM mask ($N_{voxels} = 57\,766$) generated by thresholding (cutoff = 0.2) the mean GM probability map of all 70 subjects. Then, for a given GM voxel, i, we computed its FCS using the following equation (Buckner et al. 2009; Zuo et al. 2012; Wang, Dai, et al. 2013):

$$FCS(i) = \frac{1}{N_{voxels} - 1} \sum_{j=1, j \neq i}^{N_{voxels}} z_{ij}, \quad r_{ij} > r_0 \tag{1}$$

where z_{ij} was the Fisher's Z-transformed version of correlation coefficient, r_{ij}, between voxel i and voxel j, and r_0 was a correlation threshold that was used to eliminate weak correlations possibly arising from noise (here, $r_0 = 0.2$). We also assessed the effects of different correlation thresholds on the main results, see "Validation analysis." Notably, this FCS metric is referred to as the "degree centrality" of a weighted network in graph theory (Buckner et al. 2009; Zuo et al. 2012; Wang, Dai, et al. 2013). The GM voxels with higher FCS values (>1 SD beyond the global mean) were defined as brain hubs, which are usually assumed to play central roles in the functional integrity of whole-brain networks. After the above processing, we obtained a FCS map for each subject. The spatial similarity of the FCS maps between groups was evaluated using Pearson's correlation coefficient across voxels. Given that the neighboring voxels were spatially dependent due to the physiological correlations and the smoothing preprocessing, the effective degree of freedom, df_{eff}, in the across-voxel correlation analysis was corrected to estimate the P-values (Xiong et al. 1995; Liang et al. 2013):

$$df_{eff} = \frac{N}{(FWHM_x \times FWHM_y \times FWHM_z)/v} - 2 \tag{2}$$

where v was the nominal volume of a voxel (here, $v = 3 \times 3 \times 3$ mm^3) and N was the number of voxels used in the analyses (here, $N = 57\,766$). $FWHM_x$, $FWHM_y$, and $FWHM_z$ represent the width of the Gaussian function along each of the 3 principal axes of space smoothness, respectively. Furthermore, we computed the reduced proportion of FCS, Prop(i), in the AD group relative to the HC group:

$$Prop(i) = \frac{\overline{FCS}_{AD}(i) - \overline{FCS}_{HC}(i)}{\overline{FCS}_{HC}(i)} \times 100\% \tag{3}$$

where $\overline{FCS}_{AD}(i)$ *and* $\overline{FCS}_{HC}(i)$ represent the mean FCS values of GM voxel i in the AD and HC groups, respectively. To further examine between-group differences in FCS, a general linear model (GLM) analysis was performed in a voxel-wise manner with age and gender as covariates. The statistical significance threshold was set at $P < 0.05$ and cluster size >2187 mm^3 (i.e., 81 voxels), which corresponded to a corrected $P < 0.05$ for multiple comparisons. This correction was confined within the GM mask (size: 1 559 682 mm^3) and performed by Monte Carlo simulations (Ledberg et al. 1998) using the AFNI AlphaSim program (http://afni.nimh.nih.gov/pub/dist/doc/manual/AlphaSim.pdf).

The between-group FCS difference analysis revealed regions that are disrupted in patients with AD. To further determine whether these regions showing the most significant group differences in FCS are those brain hubs with higher FCS, we generated a mean FCS map in a healthy young adult group ($n = 53$) that was obtained from a public test–retest reliability dataset (http://fcon_1000.projects.nitrc.org/indi/CoRR/html/bnu_1.html), and then computed the across-voxel spatial correlation with the between-group difference map. The correlation was computed within conjunction of the voxel sets that were defined as brain hubs (FCS > mean + 1 SD) in the healthy young group and those exhibited significant differences in FCS between AD and HC groups. The effective degree of freedom, df_{eff}, in the across-voxel correlation analysis was again corrected to estimate the P-value according to equation (2). Notably, the test–retest dataset included 2 scanning sessions and the above processing was separately performed for each session. The test–retest dataset was also used for the following reliability analysis of the FCS metric (see the "Test–retest Reliability" section) and the details of the data are shown in Supplementary Material.

The FCS metric allows us to identify brain regions that exhibit AD-related abnormalities in nodal functional connectivity. Two questions remain to be further elucidated for these regions: Exactly the connections with what regions contribute to the nodal FCS abnormalities and how regions with FCS abnormalities are topologically organized. To further address these questions, we undertook a five-step procedure as follows.

1. For each regional cluster showing significant group differences in FCS, we defined a seed region of interest (ROI) as a 4-mm-radius sphere centered on the maximal peak voxel of the cluster. Thus, we obtained 20 seed ROIs in total (see Results).
2. For each seed ROI, we performed individual functional connectivity analysis by correlating the mean time series of the seed ROI with those of all GM voxels. A Fisher's r-to-z transformation was further applied to improve the normality of the resulting correlation coefficients.
3. We used a GLM analysis to examine between-group differences in the functional connectivity maps of each seed ROI. In this step, GLM analysis was performed on individual connectivity maps with age and gender as covariates at $P < 0.001$ and cluster size > 243 mm^3, which corresponded to a corrected $P < 0.05/20$ (Bonferroni correction for 20 seed ROIs). Notably, for each seed ROI, the group difference map was restricted to positive functional connectivity maps in either the HC or AD group. Next, we defined a 4-mm radius sphere centered at each peak voxel in the difference maps as a target ROI. This procedure resulted in 27 target ROIs (see Results), whose functional connectivity with the seed ROIs differed significantly between groups.
4. Based on the above-mentioned "spreading" of connectivity analysis, we obtained 47 ROIs in total (20 seed ROIs and 27 target ROIs, without any spatial overlapping) in which AD patients exhibited disrupted FCS or relevant functional connectivity. To further ascertain how these regions showing AD-associated dysconnectivity are topologically organized, we generated a 47 × 47 correlation matrix for each subject by computing the Pearson's correlations between the time series of any pair of ROIs.
5. For each group, we thresholded ($r_0 = 0.2$) the mean correlation matrix into a weighted matrix and then performed a modular analysis using a spectral optimization algorithm (Newman 2006) in the Brain Connectivity Toolbox (http://www.indiana.edu/~cortex/connectivity.html). Moreover, we performed a GLM analysis on individual Fisher's Z-transformed version of correlation matrices to identify connectivity differences between the 2 groups. Age and gender were considered as covariates. A false discovery rate procedure was used to correct for multiple comparisons. On the basis of these analyses,

we categorized the connections showing significant group differences into intramodule (within the same functional modules) and intermodule (between different functional modules) connections.

Connectivity Distance-Related FCS Analysis

Previous studies suggested that the FCS metric is strongly associated with connectivity distance (i.e., Euclidean distance) between regions (Sepulcre et al. 2010; Liang et al. 2013; Liao et al. 2013). Thus, it would be important to examine whether AD-related changes in FCS are distance-dependent. However, there is currently no definitive distance threshold in which a given functional connectivity can be classified to be short- or long-range. Therefore, in the current study, we calculated the Euclidean distance, D_{ij}, as an approximate anatomical distance of functional connectivity between voxel i and voxel j and then divided whole-brain functional connectivity maps into 18 bins with Euclidean distances binned into 10 mm steps, ranging from 0 to 180 mm (the longest distance between voxels in the GM mask). For a given voxel, i, the FCS at the kth bin ($k = 1, 2, \ldots 18$) was computed as follows:

$$FCS(i,k) = \frac{1}{N_{voxels} - 1} \sum_{j \neq i, j \in D_{ik}} z_{ij},$$
$$r_{ij} > r_0 : D_{ik} = \{j | 10 \times (k-1) \leq D_{ij} < 10 \times k\} \quad (4)$$

where z_{ij} was the Fisher's Z-transformed version of correlation coefficient, r_{ij}, between voxel i and voxel j, N_{voxels} was the number of voxels in the GM mask (here, $N_{voxels} = 57\,766$), r_0 was 0.2 as mentioned above, and D_{ij} was the Euclidean distance between voxel i and voxel j. Thus, for each subject, a new FCS map was produced for each distance bin. To further examine between-group differences of FCS at each bin, GLM analysis was performed again in a voxel-wise manner with age and gender as covariates, and multiple comparisons were corrected using Monte Carlo simulations. Notably, the FCS maps in different distance bins contained different numbers of GM voxels, so the multiple comparison corrections were performed within the respective masks (size range: 40 608–1 559 682 mm^3). Finally, to obtain the cutoff point of short- and long-range distances using the empirical data rather than frequently employed arbitrary cutoff point at 75 mm (Achard et al. 2006; He, Chen, et al. 2007), a hierarchical clustering analysis was conducted to group the FCS maps of neighboring bins with similar spatial connectivity patterns. In this analysis, for each group, we computed the spatial correlations of FCS between different bins as follows:

$$R_{kl} = \frac{\sum_{i \in G_{kl}} (S_k^i - \overline{S_k})(S_l^i - \overline{S_l})}{\sqrt{\sum_{i \in G_{kl}} (S_k^i - \overline{S_k})^2 (S_l^i - \overline{S_l})^2}} \quad (5)$$

where S_k^i and S_l^i ($i \in G_{kl}$, G_{kl} is the overlapping of GM masks under the kth and lth bin) were the average FCS at voxel i for kth or lth bin with means of $\overline{S_k}$ and $\overline{S_l}$, respectively. After converting the spatial correlation matrix to a dissimilarity matrix (i.e., 1-correlation coefficient), we generated hierarchical cluster trees with the complete linkage clustering algorithm to hierarchical clustering analysis.

FCS-Based Classification Analysis

To determine whether the FCS metric could serve as a biomarker for distinguishing individuals with AD from the HCs, we performed a voxel-wise discriminant analysis based on the receiver operating characteristics curve approach (VDA-ROC). The statistical significance of this analysis was assessed using nonparametric permutation tests. Briefly, for each ROC classification, the class labels (e.g., AD vs. HC) were randomly permutated 10 000 times. Each time, we obtained the area under the ROC curve, and the 95th percentile points of the empirical distribution were used as critical values in a one-tailed test of whether the observed ROC curve area could occur by chance. The correction for multiple comparisons was also performed using a Monte Carlo simulation approach as described before. Notably, the discrimination analysis was also performed on short- and long-range FCS maps, respectively.

Relationship Between FCS/Modular Metrics and Cognitive Variables

To determine the relationship between nodal FCS and cognitive measures (i.e., MMSE, MoCA, ESD, AVLT, and CDT), a voxel-by-voxel GLM analysis was conducted in the AD group within the GM mask after controlling for age and gender. In the GLM analysis, we also controlled for the level of education, which is known to influence the performance on these test. Multiple comparisons were corrected using Monte Carlo simulations. In addition, we also examined the relationship between the intra- or intermodule connectivity with significant group differences and the cognitive scores in the AD group.

FCS Analysis of Very Mild and Mild AD Groups

As mentioned before, the early-stage AD group included in this study was heterogeneous, with 14 very mild AD patients (mean age, 68.93 years, SD 8.96 years; CDR = 0.5) and 18 mild AD patients (mean age, 73.06 years, SD 8.16 years; CDR = 1). To further determine whether there were different FCS patterns between these 2 AD groups, we re-performed statistical comparisons of FCS maps among the 3 groups (i.e., mild AD, very mild AD, and HC groups) using a voxel-based, one-way analysis of covariance (ANCOVA) with age and gender as covariates, followed by post hoc two-sample t-tests. Multiple comparisons were corrected using Monte Carlo simulations.

Validation Analysis

We evaluated whether our main results were influenced by GM atrophy and different preprocessing/analysis strategies (including the correlation types, correlation and connectivity density thresholds, head motion correction, spatial smoothing, and global signal removal). We also employed a public R-fMRI dataset to evaluate the test–retest reliability of the FCS measure. The relevant procedures are described as follows.

The Effects of GM Loss

Previous studies suggested that functional analysis results could potentially be influenced by structural GM differences among groups (He, Wang, et al. 2007; Oakes et al. 2007; Wang, Yan, et al. 2011). To explore the possible confounding effect of GM atrophy, we performed a voxel-based morphometry analysis on structural MRI images and took the GM density (i.e., unmodulated images) as a covariate in the FCS statistical analyses. Briefly, individual GM density maps in the standard space were obtained by a unified segmentation algorithm as described previously. After spatially smoothing with a 10-mm FWHM Gaussian kernel, voxel-wise GLM models were performed with age and gender as

covariates. Statistical significance was set at $P < 0.05$ and cluster size >12 663 mm^3, which corresponded to a corrected $P < 0.05$. Compared with the HC group, the AD group showed significant GM loss in many brain regions, especially in the medial and lateral frontal and parietal cortices and insula that exhibited AD-related disruption in FCS (see Results), indicating the necessity of correcting the GM atrophy in the R-fMRI study. We thus performed a voxel-by-voxel GLM analysis again to compare between-group differences in FCS by adding individual GM density values as an additional covariate.

The Effects of Different Preprocessing/Analysis Strategies

(1) Correlation types. Given the controversies in the treatment of negative correlations in R-fMRI network studies (Fox et al. 2009; Murphy et al. 2009; Wang, Zuo, et al. 2011), we also performed an FCS analysis including both positive and negative connections (absolute values) to assess the stability of our findings. (2) Correlation and connectivity density thresholds. While computing FCS, we used a single correlation threshold of 0.2 to eliminate potentially spurious correlations. To determine whether our main results depended on the choice of correlation threshold, we recomputed FCS maps using 5 different correlation thresholds (0, 0.1, 0.3, 0.4, and 0.5). Additionally, we also recomputed the FCS maps and performed corresponding statistical analyses under various network densities or sparsities (1%, 5%, 10%, and 20%), ensuring the same number of connections across subjects. (3) Head motion. Recent literature has suggested that head motion has a confounding effect on functional connectivity analysis (Power et al. 2012a, 2012b; Van Dijk et al. 2012; Satterthwaite et al. 2013; Yan et al. 2013). In this study, we did not find significant differences in head motion between the 2 groups [two-tailed two-sample *t*-test: $P = 0.33$ for translational, $P = 0.11$ for rotational, $P = 0.66$ for mean framewise displacement of Jenkinson (Jenkinson et al. 2002)]. Nonetheless, to exclude any possible effects of head motion, 2 analysis strategies were performed: (a) We re-analyzed FCS by including mean framewise displacement as an additional covariate (Yan et al. 2013). (b) We re-performed a 'scrubbing' procedure on the preprocessed images (Power et al. 2012a; Yan et al. 2013). For each subject, R-fMRI volumes were first censored based on a criterion of framewise displacement >0.2 mm, and the FCS analysis was then re-analyzed using these censored R-fMRI data. (4) Spatial smoothing. Given that spatial smoothing in the preprocessing steps might introduce artificial local correlations between voxels that were unrelated to their functional connections, we validated our major results without this smoothing preprocessing. (5) Global signal removal. Currently, whether global signal should be removed during R-fMRI preprocessing is controversial. Several previous studies have suggested that global signal is associated with non-neuronal activity such as respiration and should be removed (Fransson 2005; Birn et al. 2006; Chang and Glover 2009; Fox et al. 2009). However, this processing introduces widespread negative functional connectivities and thus may alter the intrinsic correlation structure of brain networks (Murphy et al. 2009; Weissenbacher et al. 2009). To explore the effects of global signal removal on our results, we re-analyzed our data without regressing out the global signal.

Test–Retest Reliability

To validate the test–retest reliability of the nodal FCS metric, we repeated the principle analyses with a public test–retest dataset (http://fcon_1000.projects.nitrc.org/indi/CoRR/html/bnu_1.html). Briefly, the dataset consists of two approximately 6.5 min R-fMRI scans that were acquired from 53 healthy young adults (male/female: 28/25; age: 19–30 years) who completed 2 MRI scan sessions within an interval of approximately 6 weeks (40.94 ± 4.51 days). The R-fMRI preprocessing and FCS calculation were all performed using the same procedures described above. We computed the intraclass correlation coefficient (Shrout and Fleiss 1979) to quantify the test–retest reliability of the FCS maps. The details of the data are presented in Supplementary Material.

Results

Whole-Brain Functional Hubs and Between-group Differences Measured by FCS

The HC group had an average of 16.35% of network density (range = 10.37–28.79%; SD = 3.53%) and the AD group had an average of 15.69% of network density (range = 11.20–21.25%; SD = 2.07%). There was no significant difference in network density between the 2 groups ($P = 0.23$). For the HC group, we observed that the brain hubs (i.e., the regions with higher FCS) were mainly distributed in several default-mode (DMN) regions including the posterior cingulate gyrus/precuneus (PCC/PCu), medial prefrontal gyrus (MPFC), and inferior parietal cortex (IPL). The insula, dorsal lateral prefrontal cortex (dlPFC), dorsal anterior cingulate cortex (dACC), postcentral gyrus (PoCG), supplemental motor area (SMA), and thalamus were also among the functional hubs (Fig. 1*A* and Supplementary Fig. 1). This pattern was largely compatible with previous R-fMRI studies in healthy young adults (Buckner et al. 2009; Liang et al. 2013; Tomasi et al. 2013). Visual inspection indicated that the spatial distributions of FCS in the AD group were very similar to those of the HC group, in spite of different strengths (Fig. 1*A* and Supplementary Fig. 1). The correlation analysis across voxels confirmed the significant spatial similarity of FCS maps between the 2 groups ($r = 0.76$, $P < 0.0001$, $df_{eff} = 24\,368$, Fig. 1*B*). Further between-group comparison analysis revealed that, compared with the HC group, the AD patients exhibited significantly decreased FCS mainly in the PCC/PCu, MPFC, IPL, PoCG, insula, dACC/SMA, dlPFC, and thalamus (corrected $P < 0.05$, Fig. 1*C* and Table 2). Notably, for most of these regions, the FCS values were reduced up to 20% in the AD group relative to the controls (Fig. 1*D*). To further explore if the brain regions showing higher FCS in the healthy population were more vulnerable to AD, we computed the spatial correlation between the FCS values of hub regions in the young healthy adult group and the between-group significant difference map (*Z* scores). High correlations were found between the 2 maps ($r = -0.22$, $P < 0.0001$, $df_{eff} = 1576$ for session 1; $r = -0.17$, $P < 0.0001$, $df_{eff} = 1576$ for session 2; Fig. 1*E*), suggesting that some hub regions of the brain networks are preferentially affected by AD.

Disrupted Hub-Related Functional Connectivity in AD

According to the above-mentioned results, we defined 20 seed ROIs showing AD-related decreases of FCS (Fig. 2 and Table 2). Furthermore, we used a "spreading" connectivity analysis to obtain 27 target ROIs showing AD-related decreases of functional connectivities with these seed ROIs (Fig. 2 and Table 3). As an example, we mapped the functional connectivity pattern of the PCC seed ROI, a 4-mm-radius sphere centered on the maximal peak voxel: x, y, z = [0, −54, 27] mm. For both the HC and AD groups, the PCC ROI was positively correlated with the MPFC, IPL, and lateral temporal gyrus (Fig. 2). The PCC functional connectivity with the MPFC was significantly lower in the AD than the HC group (corrected $P < 0.05/20$, Fig. 2), and thus, the MPFC was considered a target ROI. On the basis of these 47 ROIs, we generated a

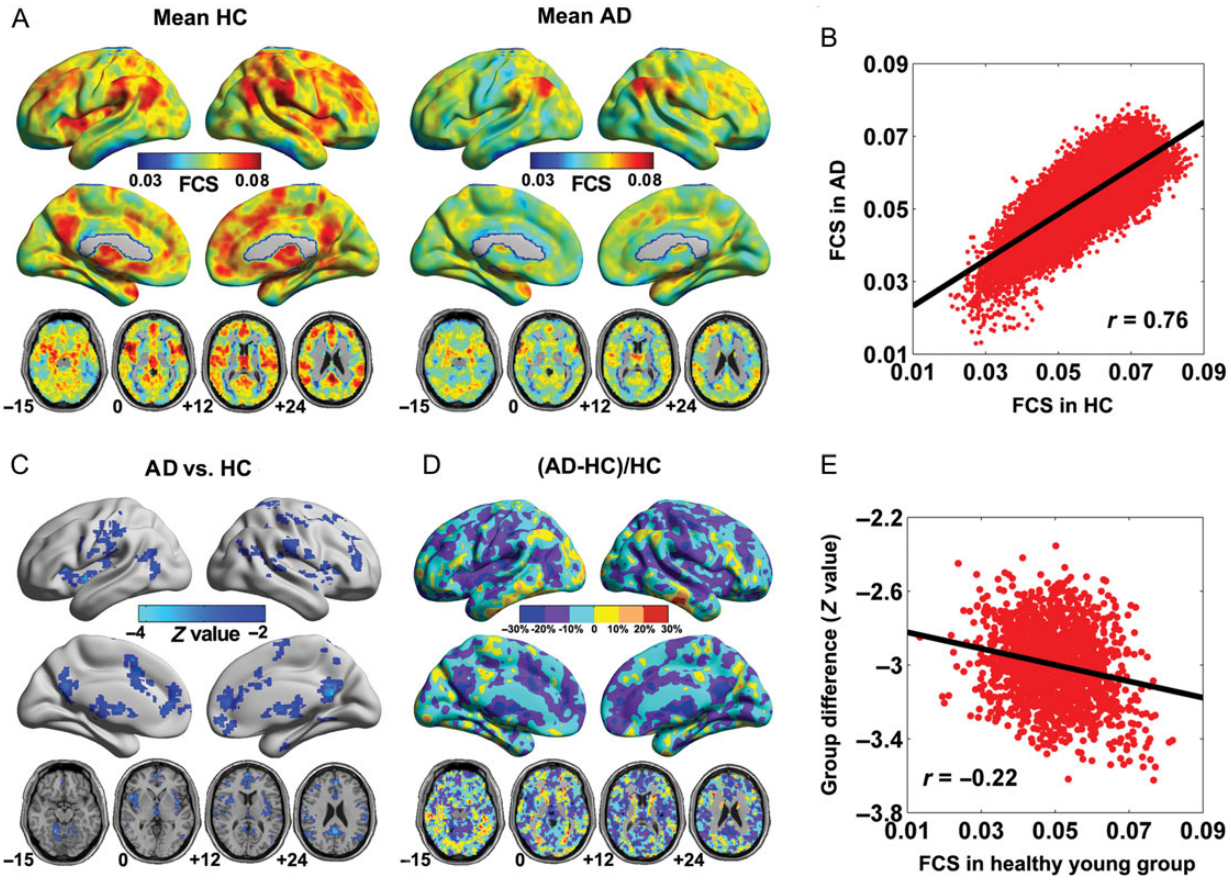

Figure 1. Within- and between-group FCS maps. (*A*) Mean FCS maps within HC and AD groups. (*B*) Scatter plot showing the across-voxel relationship between the mean FCS maps of the 2 groups. (*C*) Z-statistical difference maps between the 2 groups. (*D*) The reduced proportion of FCS in the AD group relative to the HC group. Notably, most of the regions showing AD-related changes in FCS were up to 20% lower in AD than in the control group. (*E*) Scatter plot showing the across-voxel relationship between the FCS values of hub regions in a healthy young adult group and the Z-statistical difference map. Notably, the correlation analysis was performed within a set of GM voxels that were considered hubs in the healthy young group and simultaneously showed significant differences between the AD and control groups. We resampled the FCS and Z-values into a Gaussian distribution, respectively: a mean of 0.05 and a standard deviation of 0.01 dimensionless units for FCS values, a mean of −3 and a standard deviation of 0.2 dimensionless units for Z-values. The FCS values were mapped on the cortical surface by using in-house BrainNet Viewer (Xia et al., 2013). FCS, functional connectivity strength; HC, healthy control; AD, Alzheimer's disease.

correlation matrix with 47 rows and 47 columns for each group (Fig. 3A) and further decomposed them into 3 major modules (HC: $Q_{max} = 0.471$, Z-score = 5.587; AD: $Q_{max} = 0.540$, Z-score = 1.365): the DMN, the salience network (SN), and the executive-control network (ECN; Fig. 3B and Supplementary Fig. 2). Notably, the modular structure of the HC group was highly similar to that of the AD group (Supplementary Fig. 2). Furthermore, we found that 60 ROI–ROI functional connectivities exhibited AD-related decreases ($q < 0.05$, false discovery rate correction), categorized as intramodule (53/60, 88.3%) and intermodule connections (7/60, 11.7%; Fig. 3C). These intramodule disconnections primarily belonged to the ECN (22/60, 36.6%), followed by the SN (19/60, 31.7%) and the DMN (12/60, 20%). Intermodule disconnections were located between the SN and ECN. Only one connection—between the left middle occipital gyrus and the left calcarine fissure and surrounding cortex—exhibited a significant increase in the AD group relative to the HC group.

Distance-Dependent FCS Patterns and AD-Related Abnormalities

To understand the distance-dependent FCS results, we considered the above-mentioned FCS as a full-range FCS metric. Figure 4A shows the within- and between-group FCS maps for every connectivity distance studied. We noted that the FCS maps (both the within- or between-group FCS results) showed similar patterns at the neighboring distance bins, but were very different between very short and long distances. For example, both groups exhibited higher FCS in the visual cortex and lower FCS in the IPL at the 30–40 mm distance, but the pattern was inversed at the 120–130 mm distance; the between-group differences results showed decreased FCS in AD were primarily located in the thalamus at the 30–40 mm distance, but in the PCC/PCu and MPFC at the 120–130 mm distance. Notably, the most significant AD-related FCS decreases appeared in the 100–130 mm range (Fig. 4B), suggesting that AD was mainly associated with longer distance disconnections. Additionally, we observed that several regions exhibited higher FCS in the AD group, for example, in the left fusiform gyrus at the 0–20 mm range and in the left intraparietal cortex at the 30–50 mm range (Fig. 4A,B).

We further explored the spatial similarity of the mean FCS patterns at different distances. Using a hierarchical clustering analysis, we classified the 18 FCS bins into 2 bins: 0–90 mm (short-range FCS) and 90–180 mm (long-range FCS; Fig. 4C). The clustering results were identical for the HC and AD groups. For each group, the short-range hubs (0–90 mm) were mainly located

Table 2 Regions showing FCS differences between the AD patients and HCs

Brain regions	BA	Volume (mm^3)	MNI coordinates (mm)			Z-score
			x	y	z	
PCC/PCu	31/7/23	10 206	0	−54	27	−4.13
Left IPL/PoCG/PreCG/SMG	40/2	9882	−66	−27	21	−4.07
Right SPG/PoCG	40	5346	18	−45	63	−3.89
MPFC/ACC/SMA	32/10	17 145	3	54	3	−3.89
Right MFG/SFG	6	3024	27	18	54	−3.77
Right ALC	19	6048	18	−54	−15	−3.76
Right INS/STG/SMG	13/39/47/22	17 847	39	12	6	−3.74
Left INS	13	3807	−39	0	−3	−3.60
Right MFG	9/10	5103	39	39	18	−3.35
Left ALC/PLC	N/A	4050	0	−54	−51	−3.13
Thalamus	N/A	3645	3	0	3	−3.12
Left HES/INS	13	2322	−36	−24	6	−3.05
Left MTG	39	2997	−54	−57	18	−2.95

BA, Brodmann's area; x, y, z, coordinates of primary peak locations in the MNI space; Z, statistical value of peak voxel showing FCS differences between the 2 groups; PCC/PCu, posterior cingulate cortex/precuneus; IPL/PoCG/PreCG/SMG, inferior parietal lobule/postcentral gyrus/precental gyrus/supramarginal gyrus; SPG/PoCG, superior parietal gyrus/postcentral gyrus; MPFC/ACC/SMA, medial prefrontal cortex/anterior cingulate cortex/supplementary motor area; MFG/SFG, middle frontal gyrus/superior frontal gyrus; ALC, anterior lobe of cerebellum; INS/STG/SMG, insula/superior temporal gyrus; PLC, posterior lobe of cerebellum; HES, Heschl gyrus; MTG, middle temporal gyrus.
$P < 0.05$, corrected for multiple comparisons.

in the PCC/PCu, MPFC, insula, dACC/SMA, sensorimotor, and visual cortices, whereas the long-range hubs (90–180 mm) were mainly located in the PCC/PCu, MPFC, IPL, and dlPFC (Fig. 4*D*). Notably, both the short- and long-range hub regions exhibited AD-related decreases in FCS (corrected $P < 0.05$, Fig. 4*D*).

Classification Analysis Based on Full-, Short-, and Long-Range FCS

Using the VDA-ROC analysis approach, we showed the discriminative ability of full-, short-, and long-range FCS metrics (corrected $P < 0.05$, Fig. 5). Interestingly, the brain hubs identified previously (Figs 1*A* and 4*D*, and Supplementary Fig. 1) exhibited a high power in distinguishing individuals with AD from the HCs, regardless of physical distance. Importantly, the PCC/PCu exhibited the highest classification power, with the area under the curve, sensitivity, and specificity of the ROC of 80% (95% confidence intervals: 70–90%), 84% and 66% for full-range FCS (Fig. 5*A*); 77% (95% confidence intervals: 65–87%), 81% and 66% for short-range FCS (Fig. 5*B*); and 82% (95% confidence intervals: 72–92%), 72% and 82% for long-range FCS (Fig. 5*C*), respectively.

Correlations Between the FCS/Modular Metrics and Cognitive Performance in AD

Functional Connectivity Strength

We generated the voxel-wise correlation maps between the full-, short-, and long-range FCS and behavior variables (i.e., MMSE, MoCA, ESD, AVLT, and CDT) in the AD group (corrected $P < 0.05$, Fig. 6). (1) For MMSE, there were positive correlations predominantly in the IPL with full-range FCS; in the MPFC, SMA and visual cortex with short-range FCS; and in the right PCC/PCu, IPL and dlPFC with long-range FCS. (2) For MoCA, there were positive correlations in the MPFC with full- and short-range FCS, and in the left IPL with long-range FCS. Additionally, we also observed negative correlations in the ventral part of MPFC and supramarginal gyrus with short-range FCS. (3) For ESD, we did not find any significant correlations with FCS values. (4) For AVLT, we found positive correlations in the PCC/PCu with full- and short-range FCS and no correlations with long-range FCS. (5) For CDT, there were positive correlations in the MPFC with short-range FCS, and no significant correlations with full- and long-range FCS.

Modular Connections

In the AD group, the mean functional connectivity within the ECN exhibited a positive correlation ($r = 0.49$, $P = 0.0065$) with the CDT scores. The mean functional connectivity between the SN and ECN positively correlated with the MoCA ($r = 0.38$, $P = 0.045$) and CDT ($r = 0.41$, $P = 0.028$) scores, respectively.

In summary, AD patients with lower FCS in the DMN regions (e.g., PCC/PCu, MPFC, and IPL) or lower functional connectivity between SN and ECN had lower scores in comprehensive cognitive tests (MMSE or MoCA); those with lower FCS in the PCC had impaired events memory function (lower scores on AVLT); those with lower FCS in the MPFC or lower functional connectivity within the ECN or between SN and ECN had compromised executive function (lower scores on CDT).

Disrupted Hub-Related Functional Connectivity with AD Progression

Relative to the HC group, both 2 AD groups showed commonly decreased full-range FCS in the PCC/PCu, MPFC, IPL, and insula (Fig. 7). Compared with the very mild AD group with CDR 0.5, the mild AD group with CDR 1 displayed greater reductions of FCS primarily in the PCC/PCu and IPL. These results indicated that the 2 AD groups exhibited spatially similar patterns of FCS disruptions but to different extents in several hub regions (e.g., PCC/PCu and IPL). Both short- and long- range FCS analyses yielded similar results (Fig. 7).

Validation Results

We assessed the effects of GM atrophy and different preprocessing/analysis strategies (the correlation types, correlation and connectivity density thresholds, head motion correction, spatial smoothing, and global signal removal) on our main findings as

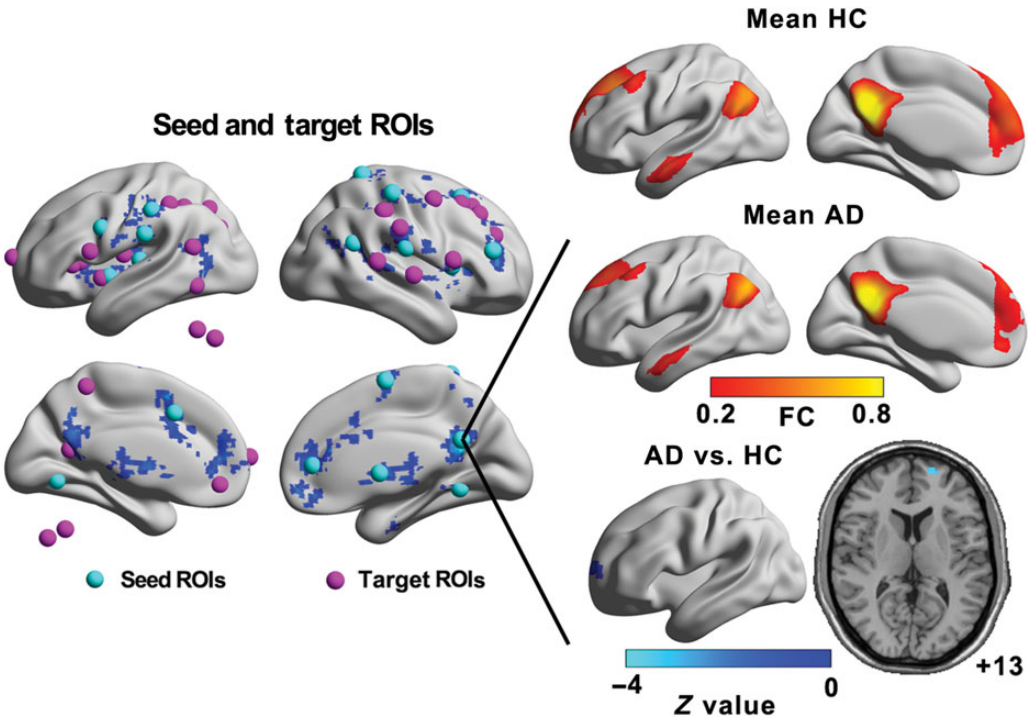

Figure 2. Definitions of seed and target ROIs. The left panel indicates the locations of the seed (cyan spheres) and target ROIs (magenta spheres). The magenta nodes outside of the brain are the regions of cerebellum. As an example, the right panel shows the mean functional connectivity maps of the PCC seed ROI (a 4-mm radius sphere centered on the maximal peak voxel: x, y, z = [0, −54, 27] mm) within the HC and AD groups and the Z-statistical differences between the 2 groups. Notably, the PCC showed significant group differences in the MPFC, which was considered a target ROI. The details of the 20 seed and 27 target ROIs are presented in Table 3. PCC, posterior cingulate cortex; MPFC, medial prefrontal cortex; HC, healthy control; AD, Alzheimer's disease.

well as the test–retest reliability of the nodal FCS metric. (1) The effects of GM loss. We observed that the AD patients showed widespread GM atrophy, with the most significant loss occurring bilaterally in the PCC/PCu, MPFC, IPL, medial temporal lobe, and insula (Fig. 8A). After taking the GM atrophy into account, we still observed the AD-related FCS decreases in the PCC/PCu, MPFC, and IPL (Fig. 8A), which was largely consistent with the main results without the GM correction (Fig. 1C). (2) The effects of correlation type. We re-generated the FCS maps using absolute correlation values including both positive and negative connections, and found that the main results preserved. For each group, the correlation analysis across voxels also confirmed a high spatial similarity between the FCS maps using the positive correlation and the FCS maps using the absolute correlation ($rs > 0.99$). The disrupted regions were mostly similar (spatial correlation, $r = 0.94$), except for the left insula and thalamus (Supplementary Fig. 3A). (3) The effects of correlation thresholds ($r_0 = 0, 0.1, 0.3, 0.4$, and 0.5) and connectivity density (density = 1%, 5%, 10%, and 20%). We found that the FCS maps of each group and the between-group difference maps under different thresholds (Supplementary Figs 3 and 4) were similar to our main results (Fig. 1). Notably, decreased FCS values in patients with AD were found in the PCC/PCu and MPFC regardless of different threshold values and thresholding approaches. (4) The effects of head motion. Using both the statistical analysis accounting for mean framewise displacement at the group-level (Yan et al. 2013; Fig. 8B) and the 'scrubbing' procedure in preprocessed images (Power et al. 2012a; Yan et al. 2013), we found that the main results in the PCC/PCu, MPFC, and IPL were not affected (Fig. 8B). Note that in this scrubbing analysis, to have sufficient time points for stable results, subjects with ≤5 min of data remaining after censoring were excluded from the analysis (8 AD patients and 11 HCs were excluded by this criterion; 51 of 70 subjects remained). (5) The effects of spatial smoothing in image preprocessing. Without spatial smoothing in image preprocessing, we observed significant group differences in the PCC and thalamus (Supplementary Fig. 5A). The between-group FCS differences in the MPFC and insula also survived the height threshold but not the extent threshold (1323 mm^3). Given that the spatial smoothing might impact distance-related FCS results, we also examined the distance-related FCS pattern without smoothing in the preprocessing. The between-group FCS differences at distance between 0 and 10 mm (Supplementary Fig. 5B) were similar to those in the main analyses at this distance range (Fig. 4A), indicating that the smoothing procedure did not influence our main findings at the short distance. Notably, the significant between-group FCS differences were also observed in longer distances (e.g., 90–130 mm), but the number of voxels showing group differences decreased without the smoothing (Supplementary Fig. 5B). (6) The effects of global signal removal. Without global signal removal, we observed that the AD group showed significantly decreased FCS in the PCC/PCu, MPFC, insula, and thalamus (Fig. 8C), which was largely consistent with our results with global signal removal. However, the lateral parietal cortices exhibited non-significant results without global signal removal. (7) Test–retest reliability. Visually, the spatial patterns of nodal FCS maps were highly similar between the 2 sessions. Pearson's correlation analysis revealed high correlation coefficient between the FCS maps in the 2 sessions ($r = 0.97$, $df_{eff} = 28\,098$, Supplementary Fig. 6). The test–retest reliability map showed spatially non-homogeneous pattern across the brain: A large amount of hub regions, including the medial and lateral frontal and parietal cortex, showed fair-to-good test–retest reliability (intraclass correlation coefficient above 0.4).

Table 3 Forty-seven ROIs

ROIs	MNI coordinates (mm)		
	x	y	z
PCC	**0**	**−54**	**27**
Left PreCG	**−51**	**6**	**31**
Left IPL	**−57**	**−26**	**46**
Left SMG	**−66**	**−27**	**21**
Right IPL	**51**	**−31**	**56**
Right SPG	**18**	**−45**	**63**
Right SMA	**3**	**−5**	**65**
Right ACC	**1**	**19**	**26**
Right MPFC	**3**	**54**	**3**
Right MFG	**27**	**18**	**54**
Right ALC	**18**	**−54**	**−15**
Right STG	**56**	**−56**	**21**
Right SMG	**57**	**−17**	**20**
Right INS	**39**	**12**	**6**
Left INS	**−39**	**0**	**−3**
Right MFG	**39**	**39**	**18**
Left ALC	**−12**	**−65**	**−11**
Right THA	**3**	**0**	**3**
Left HES	**−36**	**−24**	**6**
Left MTG	**−54**	**−57**	**18**
Left SFG	−15	60	9
Left ITG	−54	−63	−12
Left MOG	−30	−75	30
Left ANG	−33	−51	36
Left IPL	−51	−42	54
Left IFGtriang	−36	30	12
Left SPG	−24	−72	48
Right IPL	57	−30	51
Right PoCG	42	−30	42
Left PUT	−30	−9	12
Left PCu	−12	−48	57
Left ORBsup	−12	45	−12
Left PCL	−36	−72	−45
Left PCL	−30	−60	−39
Left CAL	−15	−60	15
Left INS	−42	6	−3
Left INS	−33	21	9
Right MTG	66	−39	9
Right IFGoperc	54	12	12
Left IFGoperc	−57	12	15
Right SMG	69	−21	36
Right MFG	42	0	51
Right MFG	27	36	27
Right MFG	30	30	42
Right MFG	33	18	48
Right MFG	27	27	48
Right STG	60	−12	3

Note: Bold text indicates the 20 seed ROIs derived from group FCS analysis and others indicate 27 target ROIs showing AD-related functional connectivity differences with seed ROIs.

x, y, z, coordinates of primary peak locations in the MNI space; PCC, posterior cingulate cortex; PreCG, precental gyrus; IPL, inferior parietal lobule; SMG, supramarginal gyrus; SPG, superior parietal gyrus; SMA, supplementary motor area; ACC, anterior cingulate cortex; MPFC, medial prefrontal cortex; MFG, middle frontal gyrus; ALC, anterior lobe of cerebellum; STG, superior temporal gyrus; SMG, supramarginal gyrus; INS, insula; THA, thalamus; HES, heschl gyrus; MTG, middle temporal gyrus; SFG, superior frontal gyrus; ITG, inferior temporal gyrus; MOG, middle occipital gyrus; ANG, angular gyrus; IFGtriang, inferior frontal gyrus, triangular part; PoCG, postcentral gyrus; PUT, putamen; PCu, precuneus; ORBsup, superior frontal gyrus, orbital part; PCL, posterior lobe of cerebellum; CAL, calcarine fissure and surrounding cortex; IFGoperc, inferior frontal gyrus, opercular part.

Discussion

Using R-fMRI and graph-based network analysis, we showed disrupted functional connectivity patterns in AD. Our main findings are as follows: (1) AD selectively disrupted network hub regions with higher FCS, involving the PCC/PCu, MPFC, IPL, insula, and thalamus. Importantly, this disruption was connectivity distance-dependent; (2) AD mainly disrupted within-module connections in the DMN, SN, and ECN and inter-module connections between the SN and ECN; and (3) disrupted network hub connectivity significantly correlated with patients' cognitive performance and distinguished individuals with AD from the HCs with high sensitivity and specificity.

Disrupted Brain Network Hubs in AD

An emerging feature of the connectional architecture of the human brain is that certain areas, known as hubs, act as way stations for information processing by connecting distinct, functional specialized systems (Achard et al. 2006; Sporns et al. 2007). In this study, we found that the functional hubs in the HC group were located primarily in the DMN regions, dlPFC, thalamus, and insula, consistent with previous functional network studies (Buckner et al. 2009; Tomasi and Volkow 2010; Zuo et al. 2012; Liang et al. 2013; Wang, Dai, et al. 2013). We noted that a similar hub distribution existed in the AD group, suggesting a relative preservation of the crucial roles played by these hubs. However, the patients showed the most significant FCS decreases in many hub regions, suggesting that specific brain hubs might be preferentially targeted by AD pathology. This was further evidenced by the high negative correlation between the FCS maps in the healthy young adults and group difference maps. Based on meta-analyses of published structural MRI data, Crossley et al. (2014) found that the GM lesions in AD were mainly concentrated in highly connected brain hubs such as the medial temporal and parietal regions, providing further support for our findings. The DMN regions, the core components of functional hubs, are involved in a variety of function processing, including episodic memory (Cabeza et al. 2002; Buckner 2004), a major cognitive domain impaired in early AD. A number of previous R-fMRI studies have reported abnormal spontaneous activity in the DMN in AD (Greicius et al. 2004; Wang, Zang, et al. 2006; Jones et al. 2011; Brier et al. 2012) and in the prodromal stage of AD—mild cognitive impairment (Sorg et al. 2007; Hedden et al. 2009). Beyond the DMN regions, the AD patients also exhibited decreased FCS in the dlPFC, insula, and thalamus. The dlPFC plays crucial roles in many cognitive tasks including episodic memory (Murray and Ranganath 2007), working memory, and executive function (Curtis and D'Esposito 2003); abnormal dlPFC functional connectivity has been observed in individuals at risk for AD (Liang et al. 2011). The insula is involved in somatosensation, interoception, motivation, and the maintenance of homeostasis (Deen et al. 2011). Previous studies have shown that the insula exhibits GM atrophy (Karas et al. 2003; Honea et al. 2009) and functional disconnection (Wang et al. 2007) in AD. The thalamus is a key region for integrating neural activity from widespread neocortical inputs and outputs (Postuma and Dagher 2006), and abnormal thalamic functional connectivity has been demonstrated in AD (Sanz-Arigita et al. 2010). Thus, these AD-related FCS decreases in specific brain hubs provide further support for network dysfunction in this disease.

Additionally, we also observed decreased FCS in several sensorimotor regions (PreCG, PoCG, and SMA). A structural MRI study has demonstrated a gradual loss of GM in primary sensorimotor

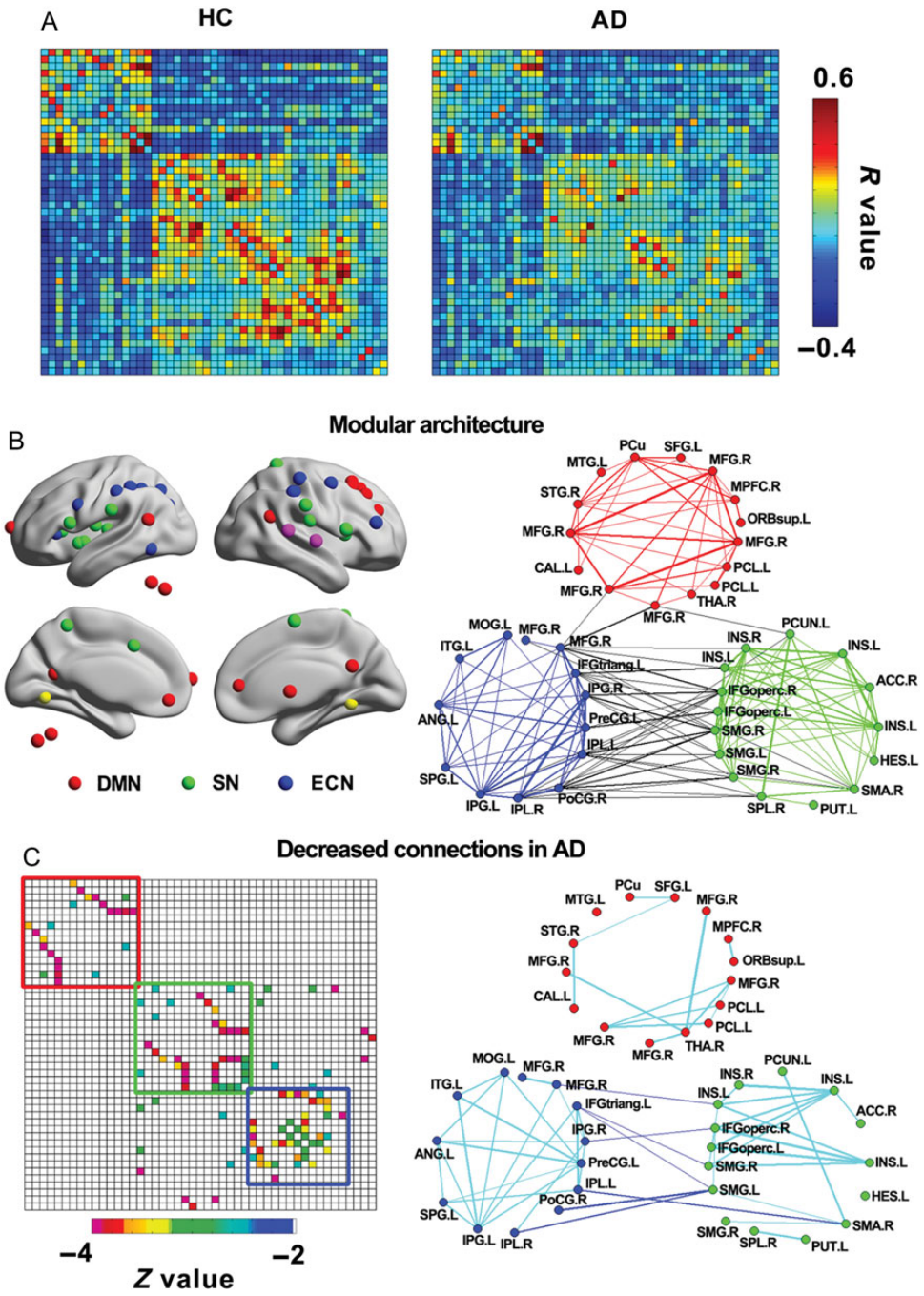

Figure 3. Modular analysis of the brain functional network. (A) Correlation matrices among 47 ROIs are shown for the HC (left panel) and AD (right panel) groups. (B) Surface (left panel) and topological (right panel) representations of the modular architecture of the brain networks in the HC group. Three modules were identified, the DMN (red colors), SN (green colors) and ECN (blue colors). The red nodes outside the brain are the regions of cerebellum. The within-module nodes and edges are marked in the same color. The intermodule connections are marked with black lines. Notably, 4 nodes (2 in magenta and 2 in yellow) on the surfaces did not belong to the DMN, SN, or ECN in the modular detection and therefore were not shown in the right panel. (C) Matrix (left panel) and topological (right panel) representations of AD-related functional connectivity decreases. Blue and cyan lines represent AD-related decreases in inter- and intramodule connections, respectively. Notably, between-group statistical comparisons were restricted to positive correlations of either the HC or AD group. DMN, default-mode network; SN, salience network; ECN, executive-control network; HC, healthy control; AD, Alzheimer's disease.

cortex that mirrors the progression of AD severity (Frisoni, Prestia, et al. 2009). Several R-fMRI studies found that the sensorimotor regions were functionally affected in early AD (Brier et al. 2012; Wang, Xia, et al. 2013; Xia et al. 2014). However, AD patients included in this study did not report any clinically evident motor deficits. The discrepancy between functional disconnection in the sensorimotor system and normal motor behaviors in the patients could be explained as brain reserve: The brain has a buffer or reserve capacity to withstand a degree of change brought about by aging and disease (Staff 2012). The biomarker model that relates disease stage to AD suggests that the synaptic dysfunction and brain structural loss are earlier than the decline of clinical performances (Jack et al. 2010; Sperling et al. 2011), providing further support for our findings.

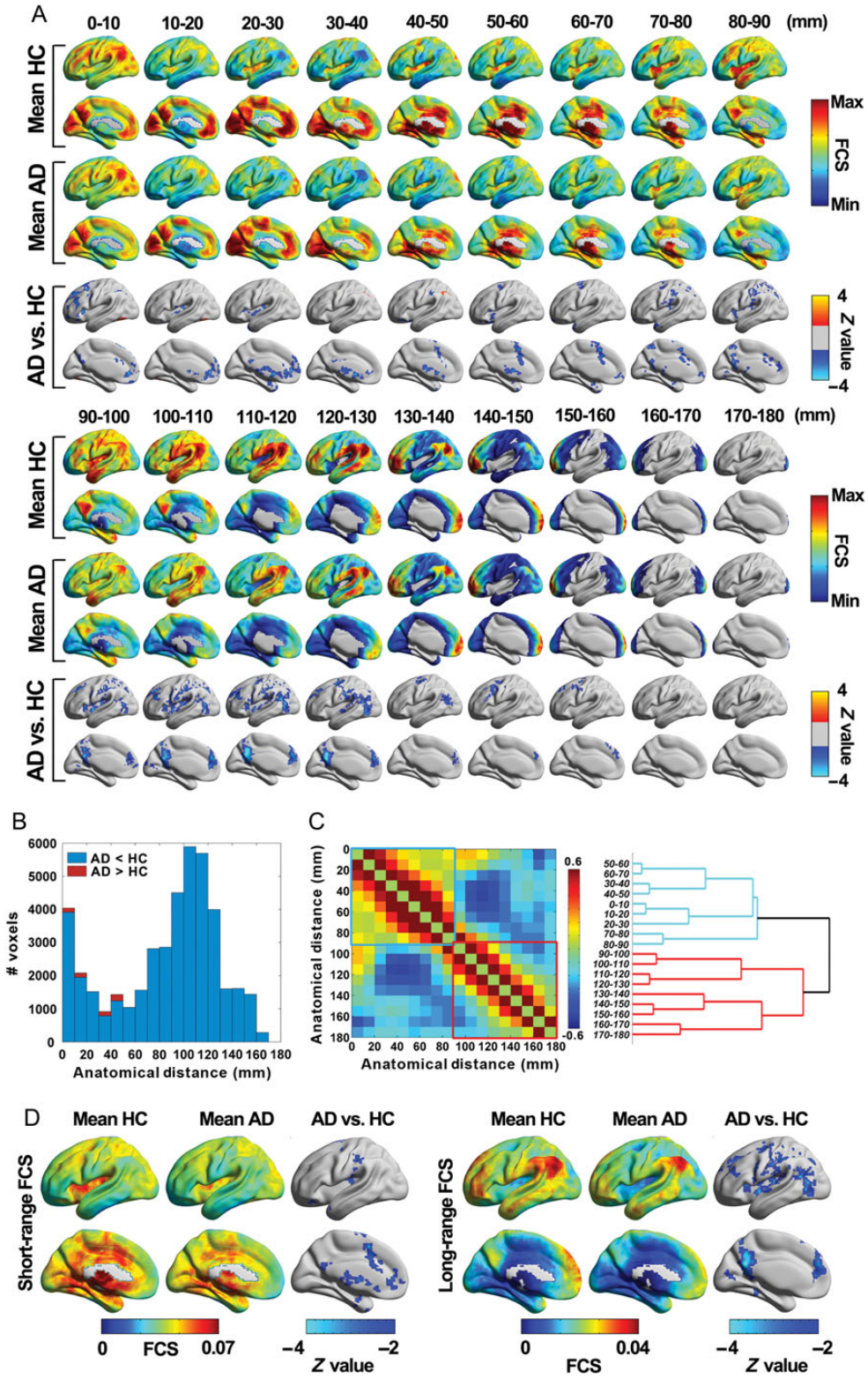

Figure 4. Distance-dependent within- and between-group FCS maps. (*A*) Within-group mean FCS maps and between-group *Z*-statistical difference maps in different distance bins. (*B*) The number of voxels showing significant group differences in FCS in different distance bins. (*C*) Hierarchical clustering analysis based on the spatial correlation map of FCS under different distance bins for the HC group. (*D*) Within-group mean FCS maps and between-group *Z*-statistical difference maps for short- and long-range FCS. FCS, functional connectivity strength; HC, healthy control; AD, Alzheimer's disease.

Many brain hubs are preferentially affected in AD, which could be explained by 2 lines of views. First, previous studies have found that the spatial pattern of typical hub regions in young healthy subjects strongly overlaps with high Aβ deposition in AD (Buckner et al. 2009) and cortical hubs are disconnected in non-demented subjects with elevated Aβ burden (Drzezga et al.

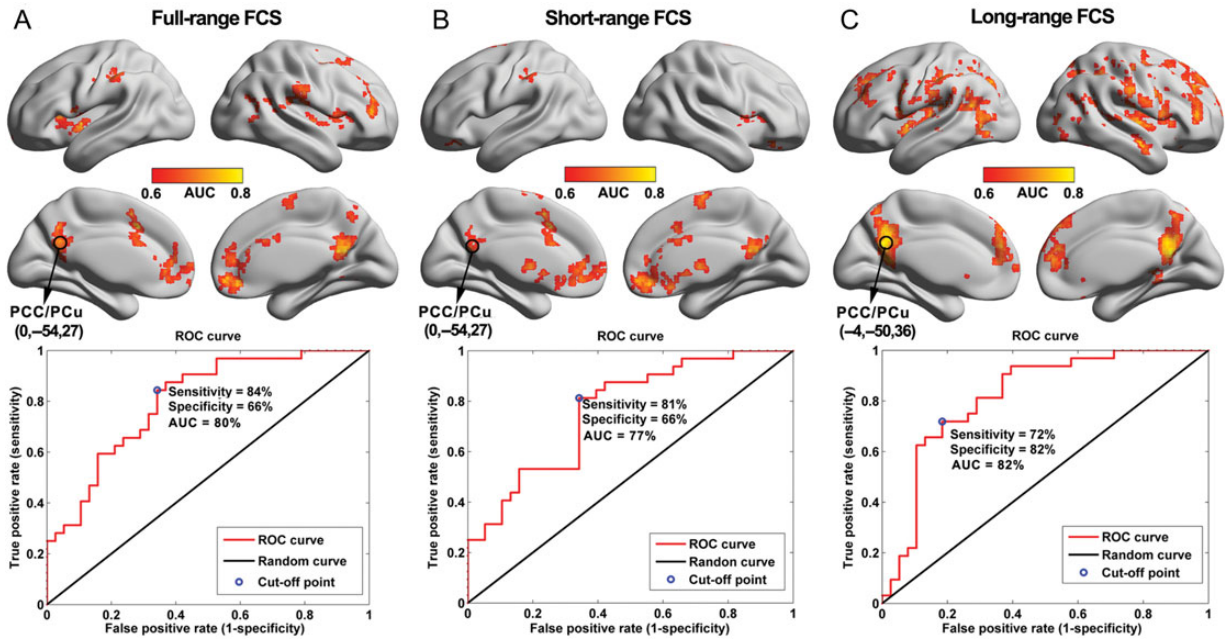

Figure 5. VDA-ROC analysis results based on the full-, short- and long-range FCS maps. The upper panel shows VDA-ROC analysis of full-range (*A*), short-range (*B*), and long-range (*C*) maps. The lower panel plots the ROC curves at the highest classification power location (i.e., PCC/PCu). FCS, functional connectivity strength; VDA-ROC, voxel-wise discriminant analysis based on the receiver operating characteristics curve approach.

2011), suggesting that increasing Aβ burden leads to functional disconnection of brain hubs. These observations conform with the Aβ-cascade hypothesis of AD that neurotoxic Aβ aggregation may lead to synaptic dysfunction and eventually synaptic loss (Hardy and Selkoe 2002; Selkoe 2008). Alternatively, a growing number of studies suggest that continuously high levels of spontaneous activity that are associated with high metabolism might lead to amyloid deposition (Bero et al. 2011; Walker and Jucker 2011). Therefore, the hub regions with higher connectivity and metabolism level might have a greater chance to have amyloid deposition. In supportive of this theory, de Haan, Mott, et al. (2012) used a computational modeling approach to demonstrate that hubs are more vulnerable to activity-dependent degeneration. In summary, there may be a bidirectional relationship between functional connectivity and Aβ deposition in AD; such a relationship has been demonstrated in mouse brain models (Bero et al. 2012). This bidirectional relationship might underlie why hub regions are preferentially affected by AD pathology.

We used R-fMRI to show AD-related network dysfunction. Notably, functional disruption in AD was also demonstrated using other neurophysiological techniques such as electroencephalograph or magnetoencephalograph (Stam et al. 2007, 2009; de Haan, van der Flier, et al. 2012). Specifically, using magnetoencephalograph data, Stam et al. (2009) examined functional connectivity changes in the resting-state brain networks in patients with AD, and found that highly connected network hubs tend to be disrupted in the patients. Also using magnetoencephalograph data, de Haan, van der Flier, et al. (2012) observed that the eigenvector centrality of the brain functional networks was the highest in the parietal regions and was disrupted in patients with AD. Convergent to the current study, these neurophysiological evidences also pointed out the notion that specific brain hubs are preferentially targeted by AD. Given the different temporal and spatial resolutions and neuronal mechanisms among electroencephalograph, magnetoencephalograph, and R-fMRI, the combination of these different techniques would be important to map a comprehensive picture of the underlying loss of network connections in AD.

Disrupted Hub-Related Connectivity and Modular Integrity in AD

We further identified AD-associated changes in the hub-relevant connectivity network. This network contains 3 main components: the DMN, the SN, and the ECN. The connections attacked by AD are involved in both intramodule connectivity within each component and intermodule connectivity between the SN and ECN. This finding is comparable with previous reports of disrupted connectivity within the DMN (Greicius et al. 2004; Brier et al. 2012), SN (Brier et al. 2012; Chen et al. 2013), and ECN (Brier et al. 2012; Li et al. 2012) in AD. Of note, 2 previous studies also reported increased connectivity within the SN (Zhou et al. 2010; Agosta et al. 2012). This discrepancy could be attributed to the different functional connectivity approaches: the 2 previous studies used independent component analysis, which identifies sets of brain regions that are separable on the basis of statistical patterns in their dynamic time series, whereas our directly identified intrinsic modules of brain networks and further examined functional connectivity patterns within modules. We also observed decreased connections between the SN and ECN. The SN is thought to play a role in recruiting relevant brain regions for the processing of sensory information (Seeley et al. 2007; Palaniyappan and Liddle 2012), and the ECN is related to the maintenance and manipulation of information and decision making in the context of goal-directed behavior (Bunge et al. 2001; Koechlin and Summerfield 2007). Therefore, we speculate that SN–ECN disconnection might lead to decreased sensory information integration, which could further accounted for the cognitive deficits in AD such as impaired judgment and disorientation.

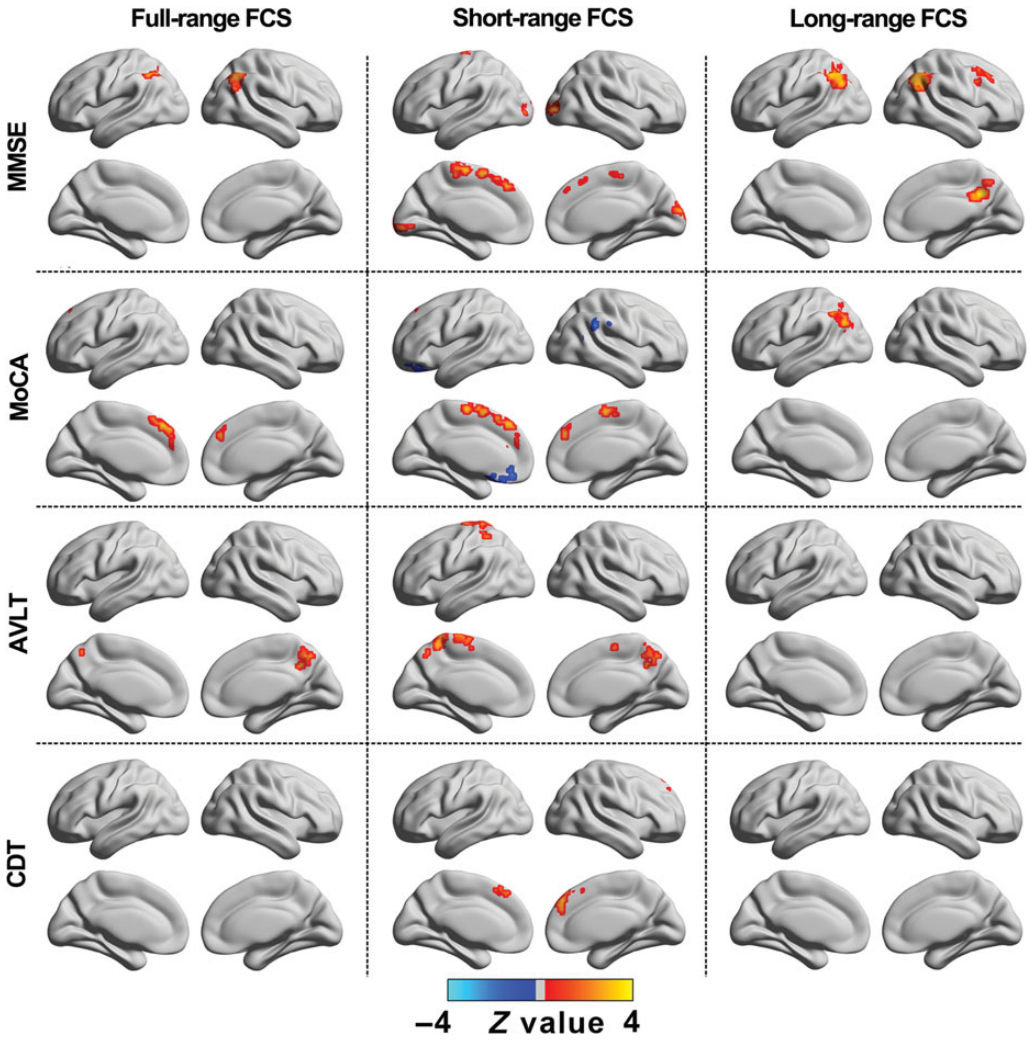

Figure 6. Correlation maps of cognitive performance and full-, short-, and long-range FCS values in the AD group. Red colors represent positive correlations and blue colors represent negative correlations. MMSE, Mini-Mental State Examination; MoCA, Montreal Cognitive Assessment; AVLT, World Health Organization–University of California–Los Angeles Auditory Verbal Learning Test; CDT, Clock Drawing Task; FCS, functional connectivity strength.

Network Hubs, Connectivity Distance, and Diagnostic Biomarkers

Disparate spatial patterns of short- versus long-range functional connections have been reported previously (Sepulcre et al. 2010; Liang et al. 2013). In the present study, long-range functional hubs were mainly located in the PCC/PCu, MPFC, IPL, and lateral frontal and temporal cortices, and these hubs exhibited significant decreases in long-range FCS in AD. These regions are involved in high-level cognitive functions such as episodic memory, executive controls, integrity of sensory information, and decision making, which are all impaired in AD. Previous studies have suggested that the long-range connections provide quick links between remote brain regions in the network (Achard et al. 2006) and play crucial roles in supporting human cognitive function by traveling across multiple modules to allow the distant hubs to act as connectors for information integration to support human cognitive function (He et al. 2009; Bullmore and Sporns 2012). Previous studies have reported AD-related disruptions in some long-distance connections involving the PCC/PCu–MPFC and bilateral homologous regions (Delbeuck et al. 2003; Stam et al. 2007; He et al. 2008; Sanz-Arigita et al. 2010; Liu et al. 2013). Therefore, we speculate that these long-range hub abnormalities might cause disrupted functional integrity between different brain systems, which could underlie the cognitive impairments in AD. This hypothesis was supported by our findings of the most significant AD-related FCS decreases appeared in the 100- to 130-mm range and significant correlations between the long-range hub FCS values in the DMN and general cognitive performances (MMSE and MoCA) in patients with AD. In this study, we observed short-range connectivity hubs mainly in the PCC/PCu, MPFC, insula, dACC/SMA, and sensorimotor and visual cortices, and these regions showed significantly decreased short-range FCS in AD. Interestingly, these disrupted short-range hubs were primarily located at the distance of 0–10 mm. This very short-range FCS might be approximately equivalent to the regional homogeneity (Zang et al. 2004). A previous study has found significant regional homogeneity decreases in the PCC/PCu and significant increases in the left fusiform in the AD patients (He, Wang, et al. 2007), which is consistent with our

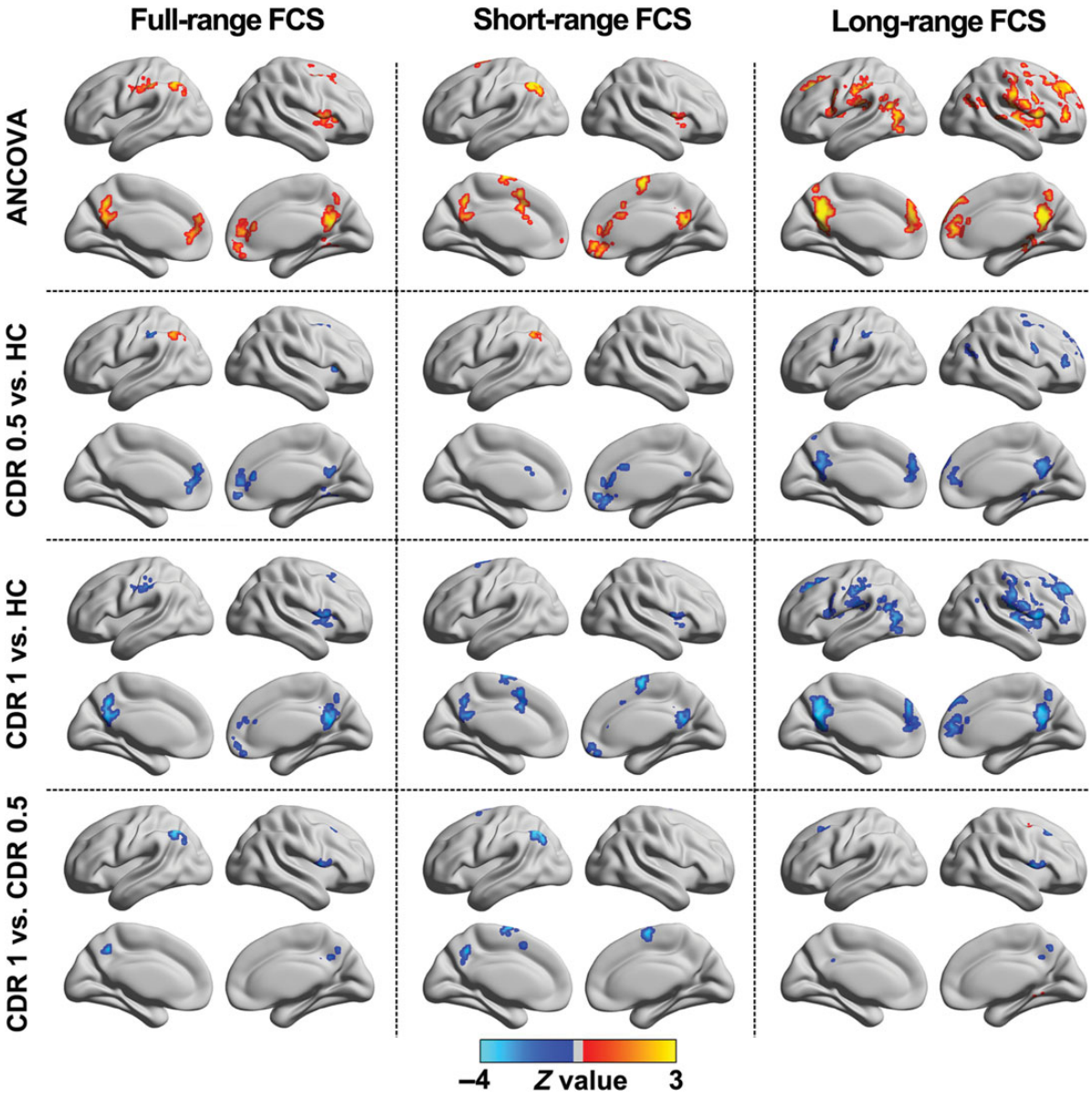

Figure 7. Disrupted FCS patterns in the very mild (CDR = 0.5) and mild (CDR = 1) AD groups when compared with the HC group. These group-based analysis results based on full-, short-, and long-range FCS maps were separately obtained by using a voxel-based, one-way analysis of covariance (ANCOVA) with age and gender as covariates, followed by post hoc two-sample *t*-tests. Notably, there were no significant differences in age, gender, and education level among the 3 groups. ANCOVA, one-way analysis of covariance; CDR, Clinical Dementia Rating; FCS, functional connectivity strength; HC, healthy control.

findings. Of note, in this study, we obtained a cutoff point (i.e., 90 mm) between short- and long-range hubs using FCS-based hierarchical clustering analysis, which captured connectivity related information and could be better than the previously employed arbitrary cutoff point of 75 mm (Achard et al. 2006; He, Chen, et al. 2007).

To further address the extent to which FCS metrics could serve as a biomarker to differentiate individuals with AD from HCs, we proposed the VDA-ROC analysis approach and found a high sensitivity and specificity in the PCC/PCu, especially for long-range FCS. The PCC/PCu is a core region of human brain structural (Hagmann et al. 2008; Gong et al. 2009) and functional (Tomasi and Volkow 2010; Liang et al. 2013) networks. Neuroimaging studies have consistently reported AD-related abnormalities in this region, such as hypometabolism (Minoshima et al. 1997), hypoperfusion (Hirao et al. 2005), amyloid deposition (Frisoni, Lorenzi, et al. 2009), cortical thinning (He et al. 2008), and functional disconnectivity (Greicius et al. 2004; Wang et al. 2007; Xia et al. 2014). These studies provide crucial evidence that the PCC/PCu FCS could be a biomarker for the early diagnosis of AD, and could also be used to evaluate the progression of the disease. Recently, many pattern recognition techniques have been widely investigated to automatically classify patients with AD or prodromal AD from healthy elders (Wang, Jiang, et al. 2006; Fan et al. 2008; Dai et al. 2012; Wee et al. 2012; Wang, Zuo, et al. 2013; Falahati et al. 2014). These approaches can be roughly grouped into 2 different categories—node-based or connectivity-based—depending on the type of features extracted from the neuroimaging data. In the first category, the features are defined as the measures of the brain nodes, such as GM volume

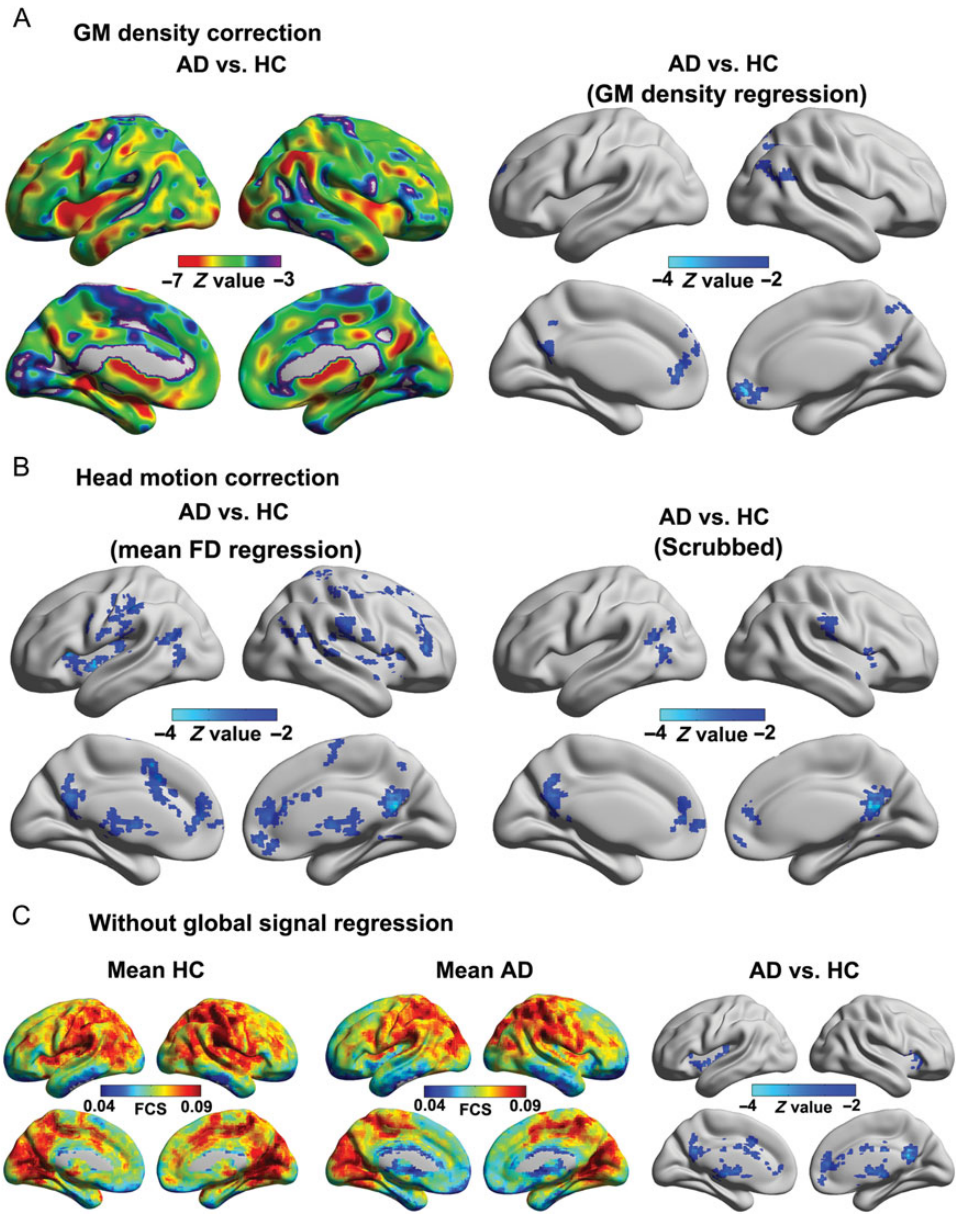

Figure 8. Validation analyses of between-group FCS differences. (*A*) The effect of GM density correction. The left panel shows Z-statistical differences in GM density between 2 groups. The right panel shows Z-statistical differences in FCS after considering GM density as additional covariates. (*B*) The effect of head motion correction. Between-group Z-statistical differences in FCS after considering the mean framewise displacement as an additional covariate (left panel) or after a 'scrubbing' procedure during preprocessing (right panel). (*C*) The effect of global signal regression. Within-group mean FCS maps and between-group Z-statistical FCS difference maps without global signal regression. GM, gray matter; FCS, functional connectivity strength; HC, healthy control; AD, Alzheimer's disease.

(Fan et al. 2008; Dai et al. 2012; Falahati et al. 2014), amplitude of low-frequency fluctuations (Dai et al. 2012), and FCS (the current study). In the second category, the features are the measures of the connectivity, such as functional correlations (Wang, Jiang, et al. 2006; Wee et al. 2012; Wang, Zuo, et al. 2013) and fiber connectivity (Wee et al. 2012) between regions. Future studies would be valuable to explore which type of features, or their combinations, are more sensitive for classifying patients with AD.

Overall, our results support the hypotheses that: (1) brain hubs with increased metabolic cost could result in amyloid plaque deposition and further lead to their functional disconnections, and (2) the disrupted brain hubs patterns in AD are connection-distance-dependent, being characterized by the disruptions of longer distance connections, which tend to consume more energy.

Further Considerations

Several issues need to be further considered. First, to address the recent concern about the spurious findings caused by head motion (Power et al. 2012a, 2012b; Van Dijk et al. 2012; Satterthwaite et al. 2013), we used both regression and scrubbing methods to validate our results, and our main findings were preserved. Nonetheless, it is worth noting that the effects of residual motion might still exist, which needs to be further validated using the optimal head motion correction methods. Second, the current

dataset is cross-sectional, therefore not allowing us to examine FCS-related dynamic changes with AD progression. Future follow-up studies are warranted to examine AD-related longitudinal changes in the network hub connectivity. Third, new criteria to diagnose AD emphasized the biomarker evidence from positron emission tomography amyloid imaging and cerebrospinal fluid. In the future, effective combination of these biomarkers (Koch et al. 2014; Myers et al. 2014) would be important to clinically diagnose AD and explore the pathophysiological mechanisms underlying these disruptions of brain hubs in AD.

Supplementary Material

Supplementary material can be found at: http://www.cercor.oxfordjournals.org/.

Funding

This work was supported by the National Key Basic Research Program of China (grant nos 2013CB837300 and 2014CB846102), the Natural Science Foundation of China (grant nos 81030028, 81225012, 31221003, 81370037, and 81401479) the Beijing Natural Science Foundation (grant no. Z111107067311036), the Beijing Funding for Training Talents (grant no. 2012D009012000003), and the Major Project of National Social Science Foundation (grant no. 11&ZD186).

Notes

We thank the 2 anonymous reviewers for their insightful comments. *Conflict of Interest*: None declared.

References

Achard S, Salvador R, Whitcher B, Suckling J, Bullmore E. 2006. A resilient, low-frequency, small-world human brain functional network with highly connected association cortical hubs. J Neurosci. 26:63–72.

Agosta F, Pievani M, Geroldi C, Copetti M, Frisoni GB, Filippi M. 2012. Resting state fMRI in Alzheimer's disease: beyond the default mode network. Neurobiol Aging. 33:1564–1578.

Alexander-Bloch AF, Vertes PE, Stidd R, Lalonde F, Clasen L, Rapoport J, Giedd J, Bullmore ET, Gogtay N. 2013. The anatomical distance of functional connections predicts brain network topology in health and schizophrenia. Cereb Cortex. 23:127–138.

Ashburner J, Friston KJ. 2005. Unified segmentation. Neuroimage. 26:839–851.

Attwell D, Laughlin SB. 2001. An energy budget for signaling in the grey matter of the brain. J Cereb Blood Flow Metab. 21:1133–1145.

Bero AW, Bauer AQ, Stewart FR, White BR, Cirrito JR, Raichle ME, Culver JP, Holtzman DM. 2012. Bidirectional relationship between functional connectivity and amyloid-β deposition in mouse brain. J Neurosci. 32:4334–4340.

Bero AW, Yan P, Roh JH, Cirrito JR, Stewart FR, Raichle ME, Lee JM, Holtzman DM. 2011. Neuronal activity regulates the regional vulnerability to amyloid-beta deposition. Nat Neurosci. 14:750–756.

Birn RM, Diamond JB, Smith MA, Bandettini PA. 2006. Separating respiratory-variation-related fluctuations from neuronal-activity-related fluctuations in fMRI. Neuroimage. 31:1536–1548.

Biswal B, Yetkin FZ, Haughton VM, Hyde JS. 1995. Functional connectivity in the motor cortex of resting human brain using echo-planar MRI. Magn Reson Med. 34:537–541.

Brier MR, Thomas JB, Snyder AZ, Benzinger TL, Zhang D, Raichle ME, Holtzman DM, Morris JC, Ances BM. 2012. Loss of intranetwork and internetwork resting state functional connections with Alzheimer's disease progression. J Neurosci. 32:8890–8899.

Buckner RL. 2004. Memory and executive function in aging and AD: multiple factors that cause decline and reserve factors that compensate. Neuron. 44:195–208.

Buckner RL, Sepulcre J, Talukdar T, Krienen FM, Liu H, Hedden T, Andrews-Hanna JR, Sperling RA, Johnson KA. 2009. Cortical hubs revealed by intrinsic functional connectivity: mapping, assessment of stability, and relation to Alzheimer's disease. J Neurosci. 29:1860–1873.

Bullmore E, Sporns O. 2009. Complex brain networks: graph theoretical analysis of structural and functional systems. Nat Rev Neurosci. 10:186–198.

Bullmore E, Sporns O. 2012. The economy of brain network organization. Nat Rev Neurosci. 13:336–349.

Bunge SA, Ochsner KN, Desmond JE, Glover GH, Gabrieli JD. 2001. Prefrontal regions involved in keeping information in and out of mind. Brain. 124:2074–2086.

Cabeza R, Dolcos F, Graham R, Nyberg L. 2002. Similarities and differences in the neural correlates of episodic memory retrieval and working memory. Neuroimage. 16:317–330.

Chang C, Glover GH. 2009. Effects of model-based physiological noise correction on default mode network anti-correlations and correlations. Neuroimage. 47:1448–1459.

Chen G, Zhang HY, Xie C, Chen G, Zhang ZJ, Teng GJ, Li SJ. 2013. Modular reorganization of brain resting state networks and its independent validation in Alzheimer's disease patients. Front Hum Neurosci. 7:456.

Collignon A, Maes F, Delaere D, Vandermeulen D, Suetens P, Marchal G. 1995. Automated multi-modality image registration based on information theory. Inf Process Med Imaging. 3:263–274.

Crossley NA, Mechelli A, Scott J, Carletti F, Fox PT, McGuire P, Bullmore ET. 2014. The hubs of the human connectome are generally implicated in the anatomy of brain disorders. Brain. 137:2382–2395.

Curtis CE, D'Esposito M. 2003. Persistent activity in the prefrontal cortex during working memory. Trends Cogn Sci. 7:415–423.

Dai Z, Yan C, Wang Z, Wang J, Xia M, Li K, He Y. 2012. Discriminative analysis of early Alzheimer's disease using multi-modal imaging and multi-level characterization with multi-classifier (M3). Neuroimage. 59:2187–2195.

D'Amelio M, Rossini PM. 2012. Brain excitability and connectivity of neuronal assemblies in Alzheimer's disease: from animal models to human findings. Prog Neurobiol. 99:42–60.

Deen B, Pitskel NB, Pelphrey KA. 2011. Three systems of insular functional connectivity identified with cluster analysis. Cereb Cortex. 21:1498–1506.

de Haan W, Mott K, van Straaten EC, Scheltens P, Stam CJ. 2012. Activity dependent degeneration explains hub vulnerability in Alzheimer's disease. PLoS Comput Biol. 8:e1002582.

de Haan W, van der Flier WM, Wang H, Van Mieghem PF, Scheltens P, Stam C. 2012. Disruption of functional brain networks in Alzheimer's disease: what can we learn from graph spectral analysis of resting-state magnetoencephalography? Brain Connect. 2:45–55.

Delbeuck X, Van der Linden M, Collette F. 2003. Alzheimer's disease as a disconnection syndrome? Neuropsychol Rev. 13:79–92.

de Reus MA, van den Heuvel MP. 2013. The parcellation-based connectome: limitations and extensions. Neuroimage. 80:397–404.

Drzezga A, Becker JA, Van Dijk KR, Sreenivasan A, Talukdar T, Sullivan C, Schultz AP, Sepulcre J, Putcha D, Greve D, et al. 2011. Neuronal dysfunction and disconnection of cortical hubs in non-demented subjects with elevated amyloid burden. Brain. 134:1635–1646.

Dubois B, Feldman HH, Jacova C, Cummings JL, Dekosky ST, Barberger-Gateau P, Delacourte A, Frisoni G, Fox NC, Galasko D, et al. 2010. Revising the definition of Alzheimer's disease: a new lexicon. Lancet Neurol. 9:1118–1127.

Dubois B, Feldman HH, Jacova C, Dekosky ST, Barberger-Gateau P, Cummings J, Delacourte A, Galasko D, Gauthier S, Jicha G, et al. 2007. Research criteria for the diagnosis of Alzheimer's disease: revising the NINCDS-ADRDA criteria. Lancet Neurol. 6:734–746.

Falahati F, Westman E, Simmons A. 2014. Multivariate data analysis and machine learning in Alzheimer's disease with a focus on structural magnetic resonance imaging. J Alzheimers Dis. 41:685–708.

Fan Y, Resnick SM, Wu X, Davatzikos C. 2008. Structural and functional biomarkers of prodromal Alzheimer's disease: a high-dimensional pattern classification study. Neuroimage. 41:277–285.

Fox MD, Raichle ME. 2007. Spontaneous fluctuations in brain activity observed with functional magnetic resonance imaging. Nat Rev Neurosci. 8:700–711.

Fox MD, Zhang D, Snyder AZ, Raichle ME. 2009. The global signal and observed anticorrelated resting state brain networks. J Neurophysiol. 101:3270–3283.

Fransson P. 2005. Spontaneous low-frequency BOLD signal fluctuations: an fMRI investigation of the resting-state default mode of brain function hypothesis. Hum Brain Mapp. 26:15–29.

Frisoni GB, Lorenzi M, Caroli A, Kemppainen N, Nagren K, Rinne JO. 2009. In vivo mapping of amyloid toxicity in Alzheimer disease. Neurology. 72:1504–1511.

Frisoni GB, Prestia A, Rasser PE, Bonetti M, Thompson PM. 2009. In vivo mapping of incremental cortical atrophy from incipient to overt Alzheimer's disease. J Neurol. 256:916–924.

Gili T, Cercignani M, Serra L, Perri R, Giove F, Maraviglia B, Caltagirone C, Bozzali M. 2011. Regional brain atrophy and functional disconnection across Alzheimer's disease evolution. J Neurol Neurosurg Psychiatry. 82:58–66.

Gong G, He Y, Concha L, Lebel C, Gross DW, Evans AC, Beaulieu C. 2009. Mapping anatomical connectivity patterns of human cerebral cortex using in vivo diffusion tensor imaging tractography. Cereb Cortex. 19:524–536.

Greicius MD, Srivastava G, Reiss AL, Menon V. 2004. Default-mode network activity distinguishes Alzheimer's disease from healthy aging: evidence from functional MRI. Proc Natl Acad Sci USA. 101:4637–4642.

Hagmann P, Cammoun L, Gigandet X, Meuli R, Honey CJ, Wedeen VJ, Sporns O. 2008. Mapping the structural core of human cerebral cortex. PLoS Biol. 6:e159.

Hardy J, Selkoe DJ. 2002. The amyloid hypothesis of Alzheimer's disease: progress and problems on the road to therapeutics. Science. 297:353–356.

He Y, Chen ZJ, Evans AC. 2007. Small-world anatomical networks in the human brain revealed by cortical thickness from MRI. Cereb Cortex. 17:2407–2419.

He Y, Chen Z, Evans A. 2008. Structural insights into aberrant topological patterns of large-scale cortical networks in Alzheimer's disease. J Neurosci. 28:4756–4766.

He Y, Evans A. 2010. Graph theoretical modeling of brain connectivity. Curr Opin Neurol. 23:341–350.

He Y, Wang J, Wang L, Chen ZJ, Yan C, Yang H, Tang H, Zhu C, Gong Q, Zang Y, et al. 2009. Uncovering intrinsic modular organization of spontaneous brain activity in humans. PLoS ONE. 4:e5226.

He Y, Wang L, Zang Y, Tian L, Zhang X, Li K, Jiang T. 2007. Regional coherence changes in the early stages of Alzheimer's disease: a combined structural and resting-state functional MRI study. Neuroimage. 35:488–500.

Hedden T, Van Dijk KR, Becker JA, Mehta A, Sperling RA, Johnson KA, Buckner RL. 2009. Disruption of functional connectivity in clinically normal older adults harboring amyloid burden. J Neurosci. 29:12686–12694.

Hirao K, Ohnishi T, Hirata Y, Yamashita F, Mori T, Moriguchi Y, Matsuda H, Nemoto K, Imabayashi E, Yamada M, et al. 2005. The prediction of rapid conversion to Alzheimer's disease in mild cognitive impairment using regional cerebral blood flow SPECT. Neuroimage. 28:1014–1021.

Honea RA, Thomas GP, Harsha A, Anderson HS, Donnelly JE, Brooks WM, Burns JM. 2009. Cardiorespiratory fitness and preserved medial temporal lobe volume in Alzheimer disease. Alzheimer Dis Assoc Disord. 23:188–197.

Jack CR Jr, Knopman DS, Jagust WJ, Shaw LM, Aisen PS, Weiner MW, Petersen RC, Trojanowski JQ. 2010. Hypothetical model of dynamic biomarkers of the Alzheimer's pathological cascade. Lancet Neurol. 9:119–128.

Jenkinson M, Bannister P, Brady M, Smith S. 2002. Improved optimization for the robust and accurate linear registration and motion correction of brain images. Neuroimage. 17:825–841.

Jones DT, Machulda MM, Vemuri P, McDade EM, Zeng G, Senjem ML, Gunter JL, Przybelski SA, Avula RT, Knopman DS, et al. 2011. Age-related changes in the default mode network are more advanced in Alzheimer disease. Neurology. 77:1524–1531.

Karas GB, Burton EJ, Rombouts SA, van Schijndel RA, O'Brien JT, Scheltens P, McKeith IG, Williams D, Ballard C, Barkhof F. 2003. A comprehensive study of gray matter loss in patients with Alzheimer's disease using optimized voxel-based morphometry. Neuroimage. 18:895–907.

Karbowski J. 2007. Global and regional brain metabolic scaling and its functional consequences. BMC Biol. 5:18.

Kelly C, Biswal BB, Craddock RC, Castellanos FX, Milham MP. 2012. Characterizing variation in the functional connectome: promise and pitfalls. Trends Cogn Sci. 16:181–188.

Kiselev VG, Hahn KR, Auer DP. 2003. Is the brain cortex a fractal? Neuroimage. 20:1765–1774.

Koch K, Myers NE, Göttler J, Pasquini L, Grimmer T, Förster S, Manoliu A, Neitzel J, Kurz A, Förstl H, et al. 2014. Disrupted intrinsic networks link amyloid-β pathology and impaired cognition in prodromal Alzheimer's disease. Cereb Cortex. doi:10.1093/cercor/bhu151.

Koechlin E, Summerfield C. 2007. An information theoretical approach to prefrontal executive function. Trends Cogn Sci. 11:229–235.

Kriegeskorte N, Cusack R, Bandettini P. 2010. How does an fMRI voxel sample the neuronal activity pattern: compact-kernel or complex spatiotemporal filter? Neuroimage. 49:1965–1976.

Ledberg A, Akerman S, Roland PE. 1998. Estimation of the probabilities of 3D clusters in functional brain images. Neuroimage. 8:113–128.

Li R, Wu X, Fleisher AS, Reiman EM, Chen K, Yao L. 2012. Attention-related networks in Alzheimer's disease: a resting functional MRI study. Hum Brain Mapp. 33:1076–1088.

Liang P, Wang Z, Yang Y, Jia X, Li K. 2011. Functional disconnection and compensation in mild cognitive impairment:

evidence from DLPFC connectivity using resting-state fMRI. PLoS ONE. 6:e22153.
Liang X, Zou Q, He Y, Yang Y. 2013. Coupling of functional connectivity and regional cerebral blood flow reveals a physiological basis for network hubs of the human brain. Proc Natl Acad Sci USA. 110:1929–1934.
Liao X-H, Xia M-R, Xu T, Dai Z-J, Cao X-Y, Niu H-J, Zuo X-N, Zang Y-F, He Y. 2013. Functional brain hubs and their test–retest reliability: a multiband resting-state functional MRI study. Neuroimage. 83:969–982.
Liu Y, Yu C, Zhang X, Liu J, Duan Y, Alexander-Bloch AF, Liu B, Jiang T, Bullmore E. 2013. Impaired long distance functional connectivity and weighted network architecture in Alzheimer's disease. Cereb Cortex. 24:1422–1435.
Lowe MJ, Mock BJ, Sorenson JA. 1998. Functional connectivity in single and multislice echoplanar imaging using resting-state fluctuations. Neuroimage. 7:119–132.
McKhann GM, Knopman DS, Chertkow H, Hyman BT, Jack CR Jr, Kawas CH, Klunk WE, Koroshetz WJ, Manly JJ, Mayeux R, et al. 2011. The diagnosis of dementia due to Alzheimer's disease: recommendations from the National Institute on Aging-Alzheimer's Association workgroups on diagnostic guidelines for Alzheimer's disease. Alzheimers Dement. 7:263–269.
Minoshima S, Giordani B, Berent S, Frey KA, Foster NL, Kuhl DE. 1997. Metabolic reduction in the posterior cingulate cortex in very early Alzheimer's disease. Ann Neurol. 42:85–94.
Morris JC. 1993. The Clinical Dementia Rating (CDR): current version and scoring rules. Neurology. 43:2412–2414.
Murphy K, Birn RM, Handwerker DA, Jones TB, Bandettini PA. 2009. The impact of global signal regression on resting state correlations: are anti-correlated networks introduced? Neuroimage. 44:893–905.
Murray LJ, Ranganath C. 2007. The dorsolateral prefrontal cortex contributes to successful relational memory encoding. J Neurosci. 27:5515–5522.
Myers N, Pasquini L, Göttler J, Grimmer T, Koch K, Ortner M, Neitzel J, Mühlau M, Förster S, Kurz A, et al. 2014. Within-patient correspondence of amyloid-β and intrinsic network connectivity in Alzheimer's disease. Brain. 137:2052–2064.
Newman ME. 2006. Modularity and community structure in networks. Proc Natl Acad Sci USA. 103:8577–8582.
Niven JE, Laughlin SB. 2008. Energy limitation as a selective pressure on the evolution of sensory systems. J Exp Biol. 211:1792–1804.
Oakes TR, Fox AS, Johnstone T, Chung MK, Kalin N, Davidson RJ. 2007. Integrating VBM into the general linear model with voxelwise anatomical covariates. NeuroImage. 34:500–508.
Palaniyappan L, Liddle PF. 2012. Does the salience network play a cardinal role in psychosis? An emerging hypothesis of insular dysfunction. J Psychiatry Neurosci. 37:17–27.
Postuma RB, Dagher A. 2006. Basal ganglia functional connectivity based on a meta-analysis of 126 positron emission tomography and functional magnetic resonance imaging publications. Cereb Cortex. 16:1508–1521.
Power JD, Barnes KA, Snyder AZ, Schlaggar BL, Petersen SE. 2012a. Spurious but systematic correlations in functional connectivity MRI networks arise from subject motion. Neuroimage. 59:2142–2154.
Power JD, Barnes KA, Snyder AZ, Schlaggar BL, Petersen SE. 2012b. Steps toward optimizing motion artifact removal in functional connectivity MRI; a reply to Carp. Neuroimage. 76:439–441.
Sanz-Arigita EJ, Schoonheim MM, Damoiseaux JS, Rombouts SA, Maris E, Barkhof F, Scheltens P, Stam CJ. 2010. Loss of 'small-world' networks in Alzheimer's disease: graph analysis of FMRI resting-state functional connectivity. PLoS ONE. 5: e13788.
Satterthwaite TD, Elliott MA, Gerraty RT, Ruparel K, Loughead J, Calkins ME, Eickhoff SB, Hakonarson H, Gur RC, Gur RE, et al. 2013. An improved framework for confound regression and filtering for control of motion artifact in the preprocessing of resting-state functional connectivity data. Neuroimage. 64:240–256.
Seeley WW, Menon V, Schatzberg AF, Keller J, Glover GH, Kenna H, Reiss AL, Greicius MD. 2007. Dissociable intrinsic connectivity networks for salience processing and executive control. J Neurosci. 27:2349–2356.
Selkoe DJ. 2006. The ups and downs of Abeta. Nat Med. 12:758–759.
Selkoe DJ. 2008. Soluble oligomers of the amyloid beta-protein impair synaptic plasticity and behavior. Behav Brain Res. 192:106–113.
Sepulcre J, Liu H, Talukdar T, Martincorena I, Yeo BTT, Buckner RL. 2010. The organization of local and distant functional connectivity in the human brain. PLoS Comput Biol. 6: e1000808.
Sheline YI, Raichle ME. 2013. Resting state functional connectivity in preclinical Alzheimer's disease. Biol Psychiatry. 74:340–347.
Shrout PE, Fleiss JL. 1979. Intraclass correlations: uses in assessing rater reliability. Psychol Bull. 86:420–428.
Smith SM, Miller KL, Salimi-Khorshidi G, Webster M, Beckmann CF, Nichols TE, Ramsey JD, Woolrich MW. 2011. Network modelling methods for fMRI. Neuroimage. 54:875–891.
Song XW, Dong ZY, Long XY, Li SF, Zuo XN, Zhu CZ, He Y, Yan CG, Zang YF. 2011. REST: a toolkit for resting-state functional magnetic resonance imaging data processing. PLoS ONE. 6: e25031.
Sorg C, Riedl V, Mühlau M, Calhoun VD, Eichele T, Läer L, Drzezga A, Förstl H, Kurz A, Zimmer C, et al. 2007. Selective changes of resting-state networks in individuals at risk for Alzheimer's disease. Proc Natl Acad Sci USA. 104: 18760–18765.
Sperling RA, Aisen PS, Beckett LA, Bennett DA, Craft S, Fagan AM, Iwatsubo T, Jack CR Jr, Kaye J, Montine TJ, et al. 2011. Toward defining the preclinical stages of Alzheimer's disease: recommendations from the National Institute on Aging-Alzheimer's Association workgroups on diagnostic guidelines for Alzheimer's disease. Alzheimers Dement. 7:280–292.
Sporns O, Honey CJ, Kotter R. 2007. Identification and classification of hubs in brain networks. PLoS ONE. 2:e1049.
Staff RT. 2012. Reserve, brain changes, and decline. Neuroimaging Clin N Am. 22:99–105.
Stam CJ, de Haan W, Daffertshofer A, Jones BF, Manshanden I, van Cappellen van Walsum AM, Montez T, Verbunt JP, de Munck JC, van Dijk BW, et al. 2009. Graph theoretical analysis of magnetoencephalographic functional connectivity in Alzheimer's disease. Brain. 132:213–224.
Stam CJ, Jones BF, Nolte G, Breakspear M, Scheltens P. 2007. Small-world networks and functional connectivity in Alzheimer's disease. Cereb Cortex. 17:92–99.
Supekar K, Menon V, Rubin D, Musen M, Greicius MD. 2008. Network analysis of intrinsic functional brain connectivity in Alzheimer's disease. PLoS Comput Biol. 4:e1000100.
Tijms BM, Wink AM, de Haan W, van der Flier WM, Stam CJ, Scheltens P, Barkhof F. 2013. Alzheimer's disease: connecting findings from graph theoretical studies of brain networks. Neurobiol Aging. 34:2023–2036.
Tomasi D, Volkow ND. 2010. Functional connectivity density mapping. Proc Natl Acad Sci USA. 107:9885–9890.

Tomasi D, Wang GJ, Volkow ND. 2013. Energetic cost of brain functional connectivity. Proc Natl Acad Sci USA. 110: 13642–13647.

Vaishnavi SN, Vlassenko AG, Rundle MM, Snyder AZ, Mintun MA, Raichle ME. 2010. Regional aerobic glycolysis in the human brain. Proc Natl Acad Sci USA. 107:17757–17762.

Van Dijk KRA, Sabuncu MR, Buckner RL. 2012. The influence of head motion on intrinsic functional connectivity MRI. Neuroimage. 59:431–438.

Vértes PE, Alexander-Bloch AF, Gogtay N, Giedd JN, Rapoport JL, Bullmore ET. 2012. Simple models of human brain functional networks. Proc Natl Acad Sci USA. 109:5868–5873.

Walker LC, Jucker M. 2011. Amyloid by default. Nat Neurosci. 14:669–670.

Wang J, Zuo X, He Y. 2010. Graph-based network analysis of resting-state functional MRI. Front Syst Neurosci. 4:16.

Wang JH, Zuo XN, Dai ZJ, Xia MR, Zhao ZL, Zhao XL, Jia JP, Han Y, He Y. 2013. Disrupted functional brain connectome in individuals at risk for Alzheimer's disease. Biol Psychiatry. 73: 472–481.

Wang JH, Zuo XN, Gohel S, Milham MP, Biswal BB, He Y. 2011. Graph theoretical analysis of functional brain networks: test-retest evaluation on short- and long-term resting-state functional MRI data. PLoS ONE. 6:e21976.

Wang K, Jiang T, Liang M, Wang L, Tian L, Zhang X, Li K, Liu Z. 2006. Discriminative analysis of early Alzheimer's disease based on two intrinsically anti-correlated networks with resting-state fMRI. Med Image Comput Comput Assist Interv. 9:340–347.

Wang K, Liang M, Wang L, Tian L, Zhang X, Li K, Jiang T. 2007. Altered functional connectivity in early Alzheimer's disease: a resting-state fMRI study. Hum Brain Mapp. 28:967–978.

Wang L, Dai Z, Peng H, Tan L, Ding Y, He Z, Zhang Y, Xia M, Li Z, Li W, et al. 2013. Overlapping and segregated resting-state functional connectivity in patients with major depressive disorder with and without childhood neglect. Hum Brain Mapp. 35:1154–1166.

Wang L, Zang Y, He Y, Liang M, Zhang X, Tian L, Wu T, Jiang T, Li K. 2006. Changes in hippocampal connectivity in the early stages of Alzheimer's disease: evidence from resting state fMRI. Neuroimage. 31:496–504.

Wang Z, Xia M, Dai Z, Liang X, Song H, He Y, Li K. 2013. Differentially disrupted functional connectivity of the subregions of the inferior parietal lobule in Alzheimer's disease. Brain Struct Funct. doi:10.1007/s00429-013-0681-9.

Wang Z, Yan C, Zhao C, Qi Z, Zhou W, Lu J, He Y, Li K. 2011. Spatial patterns of intrinsic brain activity in mild cognitive impairment and Alzheimer's disease: a resting-state functional MRI study. Hum Brain Mapp. 32:1720–1740.

Wee CY, Yap PT, Zhang D, Denny K, Browndyke JN, Potter GG, Welsh-Bohmer KA, Wang L, Shen D. 2012. Identification of MCI individuals using structural and functional connectivity networks. Neuroimage. 59:2045–2056.

Weissenbacher A, Kasess C, Gerstl F, Lanzenberger R, Moser E, Windischberger C. 2009. Correlations and anticorrelations in resting-state functional connectivity MRI: a quantitative comparison of preprocessing strategies. Neuroimage. 47: 1408–1416.

Xia M, Wang Z, Dai Z, Liang X, Song H, Shu N, Li K, He Y. 2014. Differentially disrupted functional connectivity in posteromedial cortical subregions in Alzheimer's disease. J Alzheimers Dis. 39:527–543.

Xia M, Wang J, He Y. 2013. BrainNet Viewer: a network visualization tool for human brain connectomics. PLoS ONE. 8:e68910.

Xie T, He Y. 2011. Mapping the Alzheimer's brain with connectomics. Front Psychiatry. 2:77.

Xiong J, Gao J-H, Lancaster JL, Fox PT. 1995. Clustered pixels analysis for functional MRI activation studies of the human brain. Hum Brain Mapp. 3:287–301.

Yan CG, Cheung B, Kelly C, Colcombe S, Craddock RC, Di Martino A, Li Q, Zuo XN, Castellanos FX, Milham MP. 2013. A comprehensive assessment of regional variation in the impact of head micromovements on functional connectomics. Neuroimage. 76:183–201.

Yan CG, Zang YF. 2010. DPARSF: a MATLAB toolbox for "pipeline" data analysis of resting-state fMRI. Front Syst Neurosci. 4.

Zang Y, Jiang T, Lu Y, He Y, Tian L. 2004. Regional homogeneity approach to fMRI data analysis. Neuroimage. 22:394–400.

Zhou J, Greicius MD, Gennatas ED, Growdon ME, Jang JY, Rabinovici GD, Kramer JH, Weiner M, Miller BL, Seeley WW. 2010. Divergent network connectivity changes in behavioural variant frontotemporal dementia and Alzheimer's disease. Brain. 133:1352–1367.

Zuo XN, Ehmke R, Mennes M, Imperati D, Castellanos FX, Sporns O, Milham MP. 2012. Network centrality in the human functional connectome. Cereb Cortex. 22:1862–1875.